

Elastica catastrophe machine: theory, design and experiments

ALESSANDRO CAZZOLLI, DIEGO MISSERONI, FRANCESCO DAL CORSO

DICAM, University of Trento, via Mesiano 77, I-38123 Trento, Italy

*Dedicated to our mentor and friend Davide Bigoni in honour of his 60th birthday,
for all of his invaluable teaching throughout these years and for many more to come*

Abstract

The theory, the design and the experimental validation of a catastrophe machine based on a flexible element are addressed for the first time. A general theoretical framework is developed by extending that of the classical catastrophe machines made up of discrete elastic systems. The new formulation, based on the nonlinear solution of the elastica, is enhanced by considering the concept of the universal snap surface. Among the infinite set of *elastica catastrophe machines*, two families are proposed and investigated to explicitly assess their features. The related catastrophe locus is disclosed in a large variety of shapes, very different from those generated by the classical counterpart. Substantial changes in the catastrophe locus properties, such as convexity and number of bifurcation points, are achievable by tuning the design parameters of the proposed machines towards the design of very efficient snapping devices. Experiments performed on the physical realization of the *elastica catastrophe machine* fully validate the present theoretical approach. The developed model can find applications in mechanics at different scales, for instance, in the design of new devices involving actuation or hysteresis loop mechanisms to achieve energy harvesting, locomotion, and wave mitigation.

Keywords: Nonlinear mechanics, snap mechanisms, structural instability.

1 Introduction

Catastrophe theory is a well-established mathematical framework initiated by R. Thom [31] for analyzing complex systems exhibiting instability phenomena. From its birth, concepts of this theory have been exploited over the years in several fields to provide the interpretation of sudden large changes in the configuration as the result of a small variation in the boundary conditions. Owing to its multidisciplinary application, catastrophe theory has found relevance in the mechanics of fluids, solids, and structures [11, 16, 21, 22, 26, 33, 39], but also in optics, physical chemistry, economics, biology and sociology [2, 15, 25, 32].

⁰Corresponding author: Francesco Dal Corso fax: +39 0461 282599; tel.: +39 0461 282522; web-site: <http://www.ing.unitn.it/~dalcorsf/>; e-mail: francesco.dalcorso@unitn.it

About fifty years ago, E.C. Zeeman invented and realized a simple but intriguing mechanical device [37] to illustrate for the first time concepts of catastrophe theory. The pioneering (planar) two-spring system, also known as ‘Zeeman’s catastrophe machine’, can be easily home-built by fixing two elastic rubber bands and a cardboard disk on a desktop through three drawing pins (Fig. 1, left). More specifically, the two elastic bands are tied together through a knot pinned on the cardboard disk. The other end of the first elastic band is pinned on the table while that of the second elastic band is held by hand, controlling its position within the plane. Lastly, in turn, the disk is pinned to the desktop. The resulting system has *two control parameters* (the hand position coordinates X_c and Y_c) and *one state variable* (the rotation angle ϑ of the cardboard disk). The number of equilibrium configurations for the system varies by changing the two control parameters (hand coordinates). In particular, the physical plane is split into two complementary regions separated by a symmetric concave diamond-shaped curve (with four cusps): the monostable region outside the closed curve and the bistable region inside. These two regions are respectively associated to hand position providing either a unique or two different stable equilibrium configurations (expressed by the state variable ϑ). The separating closed curve is called the *catastrophe locus* because when crossed by the hand position from inside to outside¹ provides the snapping of the system, as visual representation of the catastrophic behaviour.

Several modified versions of the Zeeman’s catastrophe machine have been proposed with the purpose to display various concepts of catastrophe theory. Different two-spring [17] and three-spring [36] systems have been shown to possibly display more (than one) separated closed curves representing the *catastrophe locus* by choosing specific design parameters. A different behaviour, the butterfly catastrophe, has been displayed when the elastic band pinned to the desktop is replaced by two identical elastic bands, with their ends symmetrically pinned to the desktop [34]. The analysis of catastrophe locus has been also extended to discrete systems with elastic hinges [6, 7]. Moreover, Zeeman’s machine has also been used to show chaotic motion [24] and its principle has been exploited to motivate the electro-mechanical instabilities of a membrane under polar symmetric conditions [23]. However, the elastic response in all of these systems has been considered to depend only on a finite number of degrees of freedom.

In this research line, the design of a catastrophe machine is extended for the first time to an elastic continuous element, namely the planar elastica, within the finite rotation regime.² The increase of the number of degrees of freedom (from finite to infinite) together with the increase in the number of kinematic boundary conditions (from two to three) requires a more complex formulation in comparison with that considered for treating the classical discrete systems.

More specifically, considering as fixed the position of one end of the elastica, the three kinematic boundary conditions X_l , Y_l (the two coordinates) and Θ_l (the rotation angle) at the other end are imposed through two control parameters. This relationship introduces a multiplicity issue for the configuration associated with the same coordinates X_l , Y_l of the final end (because of the sensitivity of the angular periodicity for the rotation angle) to be overcome

¹ Snapping occurs only for the configuration inside the bistable region which loses stability when crossing the catastrophe locus. For the classical machine this is strictly related to the sign of the rotation angle ϑ and, similarly, for the presented elastica machine to that of the curvature at the rod’s ends.

²The framework of catastrophe theory is found in the literature to be only exploited for continuous systems in investigating their equilibrium configurations as small perturbations of the undeformed one, as in the buckling problem for a pin ended rod under a lateral load [39, 40] or for a stiffened plate [19]. Differently, the catastrophe framework is here exploited for the whole set of equilibrium configurations, without any restriction on the amplitude of the related rotation field, being the analytical solutions of the Euler’s elastica equation.

for a proper representation of the catastrophe locus in the physical plane.

Furthermore, the analysis of catastrophe loci for elastica based machines requires to consider a further space, the primary kinematical space, in addition to the two spaces usually considered in the analysis of classical machines, the control parameter and the physical planes (no longer coincident here). It is shown that the catastrophe locus is provided by the projection in the physical plane of the intersection of the elastica machine set (defined by design parameters chosen for a specific machine) and the snap-back surfaces (universal for elasticae with controlled ends [8]) within the primary kinematical space.

Among the infinite set of *elastica catastrophe machines* (ECMs), two families are proposed and thoroughly investigated through the developed theoretical formulation, fully confirmed by experiments performed on a physical model (Fig. 1, right).

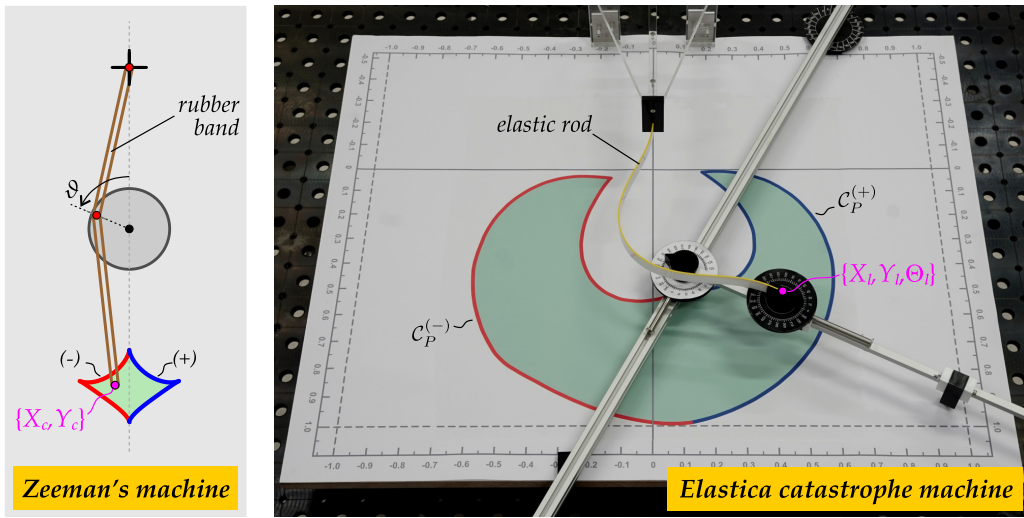


Figure 1: A sketch of the classical (discrete) catastrophe machine (left, cf. Fig. 5.1 in [25]) and a photo of the prototype realized for the proposed *elastica catastrophe machine* (right). The respective catastrophe locus C_P is reported for both machines as the union of $C_P^{(+)}$ (blue line) and $C_P^{(-)}$ (red line). Two stable equilibrium configurations exist for the elastic systems when the hand position, controlling the rubber's end coordinates X_c, Y_c (left) or the elastica's end coordinates X_l, Y_l , is within the bistable (green background) region enclosed by catastrophe locus. Differently, the stable equilibrium configuration is unique when the hand position is located within the monostable region (non-green background) defined as outside of the closed curve defining the catastrophe locus. Crossing the catastrophe locus from inside may provide snapping of the system.

An example of snapping motion displayed by the realized physical model of the *elastica catastrophe machine* (Fig. 1, right) is illustrated in Fig. 2. Two sequences of deformed configurations are shown for two different evolutions of the rod's final end position (controlled by hand). Both evolutions start from the bistable (green) domain (first column) and end to the monostable (white) domain (third column). Snapping occurs at crossing the catastrophe locus from inside to outside (second column highlighted in purple), as the elastic rod dynamically reaches the reverted stable configuration.

A parametric analysis performed by varying design parameters shows that the introduced families define catastrophe loci in a large variety of shapes, very different from those realized with classical catastrophe machines. In contrast to the classical machines, it is shown that such sets may display unexpected geometrical properties. On one hand, the number of bifurcation

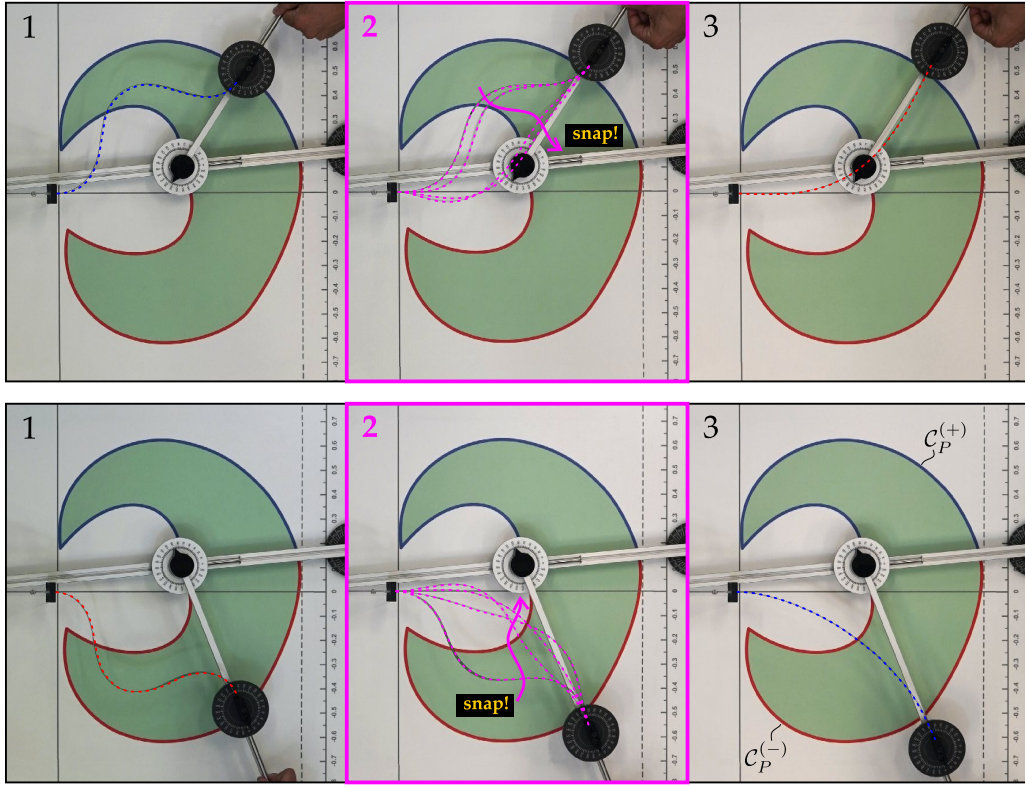


Figure 2: Evolution of the deformed configuration for two different sequences in the rod's end position controlled by hand. Snapping occurs at crossing the catastrophe locus through the blue line $\mathcal{C}_P^{(+)}$ (upper part)/red line $\mathcal{C}_P^{(-)}$ (lower part) for the elastica having positive/negative curvature at its ends. Four snapshots taken during snapping are superimposed in the second column (deformed configurations highlighted with purple dashed lines). Experiments are performed using ECM-I (with $\kappa_R = 0.5$, $\lambda_R = 0.1$, $\nu = 0$) with a carbon fiber rod by increasing the first control parameter p_1 (radial distance from the rotation point) at fixed value of p_2 (the angle Θ_l at the moving end). Deformed configurations with positive/negative curvature at its ends are highlighted with blue/red dashed line.

points along the catastrophe locus can be different than four. On the other hand, the convexity measure [41] of catastrophe locus is found to change significantly, while that of classical machines (Fig. 1, left) is usually around 0.65.³ In particular, the convex measure is found to possibly approach 1 with obtuse corners at the bifurcation points. This property facilitates reaching high-energy release snapping conditions, while these are difficult to attain in classical machines because associated with acute corner points.

The combination of the variable number of bifurcation points and the approximately unit value for the convex measure paves the way to realize very efficient snapping devices. Therefore, in addition to the interesting mechanical and mathematical features with reference to catastrophe theory in combination with snapping mechanisms [1, 4, 5, 9, 10, 13, 28, 29, 30], the proposed model may find application in the design of cycle mechanisms for actuation and dissipation devices towards energy harvesting, locomotion and wave mitigation [3, 12, 14, 18, 20, 27, 35].

³Convex catastrophe loci can be found for force controlled discrete systems [36]. Nevertheless, convex catastrophe loci are not observed for classical catastrophe machines under displacement control.

2 Equilibrium configurations for the elastica and the universal snap surface

The equilibrium configurations and the concept of universal snap surface are recalled for the *inextensible planar elastica* of length l and lying within the $X - Y$ plane, which models the flexible element composing the *elastica catastrophe machine*. Considering the flexible element (the rod) kinematically constrained at its two ends, the following six boundary conditions are imposed

$$\begin{aligned} X(s=0) &= X_0, & Y(s=0) &= Y_0, & \Theta(s=0) &= \Theta_0, \\ X(s=l) &= X_l, & Y(s=l) &= Y_l, & \Theta(s=l) &= \Theta_l, \end{aligned} \quad (1)$$

where $s \in [0, l]$ denotes arc length along the rod, X and Y the Cartesian coordinates and Θ the anticlockwise rotation evaluated with respect to the X axis. The inextensibility of the elastic rod constrains the distance d between its two ends to satisfy the following kinematic compatibility condition

$$d(X_0, Y_0, X_l, Y_l) = \sqrt{(X_l - X_0)^2 + (Y_l - Y_0)^2} \leq l. \quad (2)$$

The inextensibility assumption also introduces the dependence of the coordinate fields $X(s)$ and $Y(s)$ on the rotation field $\Theta(s)$ through the following differential relations

$$X'(s) = \cos \Theta(s), \quad Y'(s) = \sin \Theta(s), \quad (3)$$

where the symbol $'$ denotes the derivative with respect to the curvilinear coordinate s .

Given the six boundary conditions (1), the deformed configuration of the elastic rod at equilibrium is described by

$$\begin{cases} X(s) = X_0 + \frac{X_l - X_0}{d} C(s)l - \frac{Y_l - Y_0}{d} D(s)l, \\ Y(s) = Y_0 + \frac{X_l - X_0}{d} D(s)l + \frac{Y_l - Y_0}{d} C(s)l, \\ \Theta(s) = \arctan \left[\frac{Y_l - Y_0}{X_l - X_0} \right] + \beta + 2\zeta(s), \end{cases} \quad (4)$$

where β is related to the inclination of the reaction force at the ends, measured as anti-clockwise angle with respect to the straight line connecting the two clamps, while

$$C(s) = A(s) \cos \beta + B(s) \sin \beta, \quad D(s) = A(s) \sin \beta - B(s) \cos \beta. \quad (5)$$

In the case when the number m of inflection points along the rod is null, the three functions $\zeta(s)$, $A(s)$, and $B(s)$ are given by

$$\begin{cases} \zeta(s) = \operatorname{am} \left(\frac{s}{l} (F(\zeta_l, \xi) - F(\zeta_0, \xi)) + F(\zeta_0, \xi), \xi \right), \\ A(s) = \frac{2}{\xi^2} \frac{\mathcal{E} \left(\frac{s}{l} (F(\zeta_l, \xi) - F(\zeta_0, \xi)) + F(\zeta_0, \xi), \xi \right) + \mathcal{E}(F(\zeta_0, \xi), \xi)}{F(\zeta_l, \xi) - F(\zeta_0, \xi)} - \frac{2 - \xi^2 s}{\xi^2 l}, \\ B(s) = \frac{2}{\xi^2} \frac{\operatorname{dn} \left(\frac{s}{l} (F(\zeta_l, \xi) - F(\zeta_0, \xi)) + F(\zeta_0, \xi), \xi \right) - \operatorname{dn}(F(\zeta_0, \xi), \xi)}{F(\zeta_l, \xi) - F(\zeta_0, \xi)}. \end{cases} \quad (6)$$

Differently, when at least one inflection point is present ($m \neq 0$),

$$\begin{cases} \zeta(s) = \arcsin \left[\eta \operatorname{sn} \left(\frac{s}{l} (F(\omega_l, \eta) - F(\omega_0, \eta)) + F(\omega_0, \eta), \eta \right) \right], \\ A(s) = 2 \frac{\mathcal{E} \left(\frac{s}{l} (F(\omega_l, \eta) - F(\omega_0, \eta)) + F(\omega_0, \eta), \eta \right) - \mathcal{E}(F(\omega_0, \eta), \eta)}{F(\omega_l, \eta) - F(\omega_0, \eta)} - \frac{s}{l}, \\ B(s) = 2\eta \frac{\operatorname{cn} \left(\frac{s}{l} (F(\omega_l, \eta) - F(\omega_0, \eta)) + F(\omega_0, \eta), \eta \right) - \operatorname{cn}(F(\omega_0, \eta), \eta)}{F(\omega_l, \eta) - F(\omega_0, \eta)}. \end{cases} \quad (7)$$

In the aforementioned equations F is *Jacobi's incomplete elliptic integral of the first kind*, \mathcal{E} *Jacobi's epsilon function*, E *Jacobi's incomplete elliptic integral of the second kind*, 'sn' *Jacobi's sine amplitude function*, 'cn' *Jacobi's cosine amplitude function*, 'dn' *Jacobi's elliptic function*, and 'am' *Jacobi's amplitude function*,

$$\begin{aligned} F(\varphi, k) &= \int_0^\varphi \frac{d\phi}{\sqrt{1 - k^2 \sin^2 \phi}}, \quad E(\varphi, k) = \int_0^\varphi \sqrt{1 - k^2 \sin^2 \phi} d\phi, \quad \mathcal{E}(\varphi, k) = E(\operatorname{am}(\varphi, k), k), \\ \operatorname{sn}(u, k) &= \sin(\operatorname{am}(u, k)), \quad \operatorname{cn}(u, k) = \cos(\operatorname{am}(u, k)), \\ \varphi &= \operatorname{am}\left(F(\varphi, k), k\right), \quad \operatorname{dn}(u, k) = \sqrt{1 - k^2 \operatorname{sn}^2(u, k)}. \end{aligned} \quad (8)$$

Moreover, the parameters ζ_0 , ζ_l , η , ω_0 , and ω_l appearing in eqns (6) and (7) are given by

$$\begin{aligned} \zeta_0 &= \frac{\Theta_0 + \beta}{2} - \frac{1}{2} \arctan \left[\frac{Y_l - Y_0}{X_l - X_0} \right], \quad \zeta_l = \frac{\Theta_l + \beta}{2} - \frac{1}{2} \arctan \left[\frac{Y_l - Y_0}{X_l - X_0} \right], \quad \eta = \left| \sin \hat{\zeta} \right|, \\ \omega_0 &= \arcsin \left(\frac{\sin \zeta_0}{\eta} \right), \quad \omega_l = (-1)^m \arcsin \left(\frac{\sin \zeta_l}{\eta} \right) + (-1)^j m\pi, \end{aligned} \quad (9)$$

with $\hat{\zeta} = \zeta(\hat{s})$, \hat{s} being the smallest curvilinear coordinate s corresponding to an inflection point, $\Theta'(\hat{s}) = 0$, and the parameter j related to the sign of curvature at $s = 0$ (corresponding to $j = 0$ if $\Theta'(s = 0) > 0$, and $j = 1$ if $\Theta'(s = 0) < 0$), while ξ is a parameter restricted to

$$\xi \in \left[0, \sqrt{\frac{2}{1 - \min_{s \in [0, l]} \{\cos 2\zeta(s)\}}} \right]. \quad (10)$$

The position fields $X(s)$, $Y(s)$, and $\Theta(s)$, eqn (4), define the configuration taken by the elastica when constrained by the two ends. In particular, the equilibrium configuration (in general non-unique) can be characterized once the two unknown parameters (ξ and β for $m = 0$, η and β for $m \neq 0$) are evaluated for a given set of kinematical boundary conditions, eqn (1). The pair(s) of these parameters can be obtained by solving the following nonlinear system,

$$\begin{cases} C(l) = \frac{d}{l}, \\ D(l) = 0. \end{cases} \quad (11)$$

Towards the stability analysis of a specific equilibrium configuration related to the six boundary conditions $X_0, X_l, Y_0, Y_l, \Theta_0, \Theta_l$, it is instrumental to refer to the following three primary kinematical quantities: the distance d , eqn (2), and the angles θ_A and θ_S , respectively defined as the antisymmetric and symmetric parts of the imposed end rotations,

$$\theta_A = \frac{\Theta_l + \Theta_0}{2} - \arctan \left[\frac{Y_l - Y_0}{X_l - X_0} \right], \quad \theta_S = \frac{\Theta_l - \Theta_0}{2}. \quad (12)$$

In particular, the triads $\{d, \theta_A, \theta_S\}$ can be related to a unique or two different stable configurations through a function $S_K(d, \theta_A, \theta_S)$ as [8]

$$\begin{aligned} S_K(d, \theta_A, \theta_S) > 0 & \Leftrightarrow \text{monostable domain: one stable configuration,} \\ S_K(d, \theta_A, \theta_S) < 0 & \Leftrightarrow \text{bistable domain: two stable configurations.} \end{aligned} \quad (13)$$

Universal snap surface. The transition between the bistable and monostable domains (13) occurs for the set of critical conditions of snap-back for one of the two stable configurations, differing by the sign of curvature at the two ends. Such a condition can be represented through the concept of *universal snap surface* (restricted here to type 1 only [8]), which can be expressed in the following implicit form

$$S_K(d, \theta_A, \theta_S) = 0 \quad \Leftrightarrow \quad \text{one stable and one critical configuration at snap,} \quad (14)$$

The equation (14) defines a closed surface within the space of the primary kinematical quantities $\{d, \theta_A, \theta_S\}$, with two planes of symmetry defined by $\theta_A = 0$ and $\theta_S = 0$ (Fig. 3, left).⁴ The intersection of the surface S_K with its two symmetry planes provides two closed curves representing the whole set of pitchfork bifurcation points. More specifically, the pitchfork bifurcation points are distinguished as *supercritical* or *subcritical*, the former corresponding to the intersection curve with $\theta_S = 0$ and the latter with $\theta_A = 0$. Therefore, the generic planar section of S_K at fixed values of d has shape and physical meaning definitely similar to those of the catastrophe locus of the classical Zeeman machine (see Fig. 1 left) having two canonical and two dual cusps, see [8] and [25]. A critical configuration with a certain sign of curvature at the two ends is characterized by symmetric angle θ_S with the same sign. Due to the symmetry properties described above, the implicit function $S_K(d, \theta_A, \theta_S)$ can be described through two single value functions $\theta_S^{sb(+)}$ and $\theta_S^{sb(-)}$ of the two primary kinematical quantities d and θ_A ,

$$\theta_S^{sb(+)} = \theta_S^{sb(+)}(d, \theta_A), \quad \theta_S^{sb(-)} = \theta_S^{sb(-)}(d, \theta_A), \quad (15)$$

where the sign enclosed by the superscript parentheses is related to the sign of curvature at the two ends before snapping, related to the parameter j in eqn (9). This sign is also coincident with that of the symmetric angle of the snapping configuration. Furthermore, symmetry properties lead to the following conditions

$$\theta_S^{sb(+)}(d, \theta_A) = \theta_S^{sb(+)}(d, -\theta_A) = -\theta_S^{sb(-)}(d, \theta_A) = -\theta_S^{sb(-)}(d, -\theta_A). \quad (16)$$

⁴It is noted that a type 1 snapping configuration is always related to an elastica with two inflection points, $m = 2$, which snaps towards another elastica with two inflection points. Therefore, each configuration at snapping displays the same curvature the sign at both ends, changing sign from just before to just after the snap mechanism.

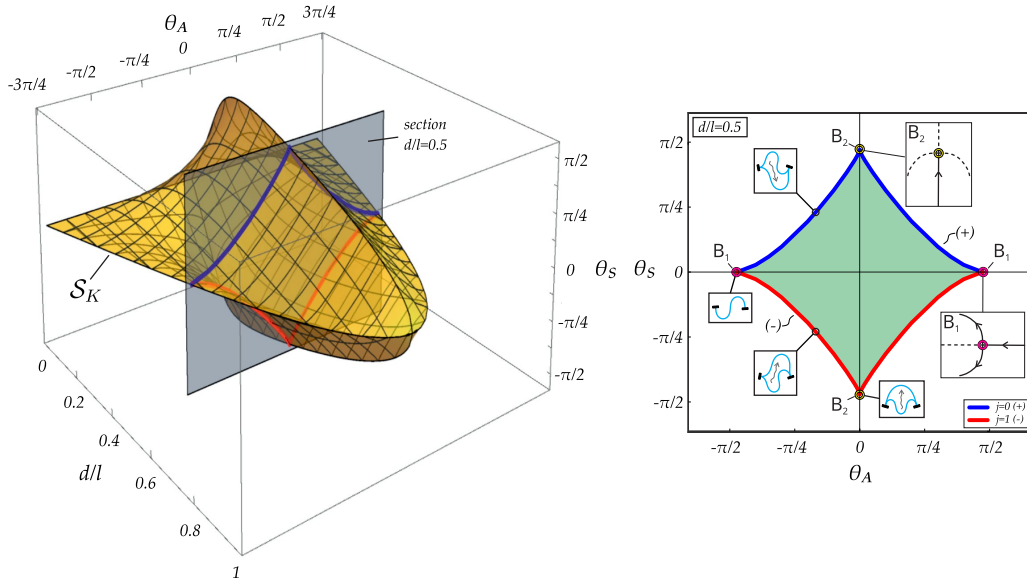


Figure 3: (Left) Universal snap surface S_K (type 1) within the space of the primary kinematical quantities $\{d, \theta_A, \theta_S\}$ and its section with the plane $d = 0.5l$. (Right) Snap surface section for $d = 0.5l$ as thick closed curve within the plane $\theta_A - \theta_S$ composed by blue (+) and red (-) parts. The blue (red) part refers to snapping configurations with positive $j = 0$ (negative $j = 1$) curvature at both ends. The bistable (monostable) domain is reported as the green (white) region inside (outside) the closed curve. The deformed shapes of the elastica before and after snapping are reported as insets for some critical condition along the closed curve are reported. The two cusps B_1 (B_2) are supercritical (subcritical) pitchfork bifurcations, and are associated with a non-snapping (a snapping) configuration.

3 Theoretical framework for *elastica catastrophe machines*

The aim of this section is to develop the theoretical framework for the realization of the *elastica catastrophe machine*. For the sake of simplicity, the initial coordinate of the elastic rod, $s = 0$, is considered fixed and taken as the origin of the reference system $X - Y$ and with tangent parallel to the X -axis, so that

$$X_0 = Y_0 = \Theta_0 = 0. \quad (17)$$

It follows that the three primary kinematical quantities, eqn (12) can be expressed as functions (overtilde symbol) of the position at the final coordinate ($s = l$) only,

$$d = \tilde{d}(X_l, Y_l), \quad \theta_A = \tilde{\theta}_A(X_l, Y_l, \Theta_l), \quad \theta_S = \tilde{\theta}_S(\Theta_l), \quad (18)$$

which simplify as⁵

$$\tilde{d}(X_l, Y_l) = \sqrt{X_l^2 + Y_l^2}, \quad \tilde{\theta}_A(X_l, Y_l, \Theta_l) = \frac{\Theta_l}{2} - \arctan \left[\frac{Y_l}{X_l} \right], \quad \tilde{\theta}_S(\Theta_l) = \frac{\Theta_l}{2}, \quad (19)$$

Relations (19) can be inverted to provide the position at the final coordinate ($s = l$) as a function (hat symbol) of the primary kinematical quantities

$$\hat{X}_l(d, \theta_A, \theta_S) = d \cos(\theta_S - \theta_A), \quad \hat{Y}_l(d, \theta_A, \theta_S) = d \sin(\theta_S - \theta_A), \quad \hat{\Theta}_l(\theta_S) = 2\theta_S. \quad (20)$$

⁵Details about overcoming periodicity issues inherent to the trigonometric function \arctan are reported in Section ?? of the Supplementary Material.

The definition of a (catastrophe) machine leads to the introduction of control and design parameters, respectively collected in the two vectors $\mathbf{p} = \{p_1, \dots, p_M\}$ and $\mathbf{q} = \{q_1, \dots, q_N\}$ (with $M, N \in \mathbb{N}$). In particular, \mathbf{p} is the fundamental vector collecting the degrees of freedom of the considered machine. Thus, the position of the rod at the final curvilinear coordinate ($s = l$) can be also described as functions (overbar symbol) of such parameters as

$$X_l = \bar{X}_l(\mathbf{p}, \mathbf{q}), \quad Y_l = \bar{Y}_l(\mathbf{p}, \mathbf{q}), \quad \Theta_l = \bar{\Theta}_l(\mathbf{p}, \mathbf{q}), \quad (21)$$

and similarly, considering eqns (19) and (21), the three primary kinematical quantities d, θ_A and θ_S as

$$d = \bar{d}(\mathbf{p}, \mathbf{q}), \quad \theta_A = \bar{\theta}_A(\mathbf{p}, \mathbf{q}), \quad \theta_S = \bar{\theta}_S(\mathbf{p}, \mathbf{q}). \quad (22)$$

Although both the control and design parameters affect the elastica configuration, a distinction is made being the former varied at fixed values of the latter.

In the following, towards the geometrical representation of the *catastrophe locus* (namely, the critical conditions providing snapping for the elastica) within the physical plane $X - Y$, the number of control parameters is taken as $M = 2$, so that $\mathbf{p} = \{p_1, p_2\}$.

Finally, it is assumed that the relations (21) and (22) can be inverted, thus obtaining

$$p_j = \tilde{p}_j(X_l, Y_l, \Theta_l, \mathbf{q}) \quad j = 1, 2, \quad (23)$$

and

$$p_j = \hat{p}_j(d, \theta_A, \theta_S, \mathbf{q}) \quad j = 1, 2, \quad (24)$$

respectively. A generic configuration of the elastica can be therefore represented by the three equivalent parametrisations of the boundary conditions, namely i) by the two control parameters $\{p_1, p_2\}$, ii) by the three coordinates of the rod's final end $\{X_l, Y_l, \Theta_l\}$ or iii) by the three primary kinematical quantities $\{d, \theta_A, \theta_S\}$. This discrepancy in the number of the required parameters suggests that one of the coordinates of the triads $\{X_l, Y_l, \Theta_l\}$ or $\{d, \theta_A, \theta_S\}$ might be expressed as a function of the remaining two. Section ?? of the Supplementary Material is devoted to the development of such statement.

3.1 Three spaces for representing the catastrophe locus

In light of the above, the complete understanding of the principles underlying the present catastrophe machine requires to consider the projection of the controlled end's configuration within the three different spaces,

C : the control parameter plane $p_1 - p_2$;

K : the primary kinematical quantities space $d - \theta_A - \theta_S$;

P : the physical space $X_l - Y_l - \Theta_l$, where the rotational coordinate Θ_l (possibly even more than one) is condensed to the physical plane $X_l - Y_l$.

The need of these three different representations and the (unavoidable) projection of the rotational coordinate Θ_l to the physical plane $X_l - Y_l$ are the new constituents of the *elastica catastrophe machine* with respect to the classical one [37, 38], where the control plane coincides with the physical one and the kinematical space is not needed. Furthermore, differently from the classical catastrophe machine, the values of the control parameters p_1 and p_2 , kinematical

quantities d , θ_A , and θ_S , and the end's coordinates X_l , Y_l , and Θ_l are here restricted by the inextensibility constraint, eqn (2), so that their variation is limited to the ‘inextensibility set’ \mathcal{I} , which is defined in the three different spaces as

$$\begin{aligned}\mathcal{I}_C &:= \{\mathbf{p} \in \mathbb{R}^2 \mid 0 \leq \bar{d}(\mathbf{p}, \mathbf{q}) \leq l\}, \\ \mathcal{I}_K &:= \{\{d, \theta_A, \theta_S\} \in \mathbb{R}^3 \mid 0 \leq d \leq l\}, \\ \mathcal{I}_P &:= \{\{X_l, Y_l\} \in \mathbb{R}^2 \mid 0 \leq \tilde{d}(X_l, Y_l) \leq l\}.\end{aligned}\tag{25}$$

In order to minimize the presence of self-intersecting configurations⁶ for the elastica, the symmetric θ_S and antisymmetric θ_A angles are considered to be restricted by

$$\{|\theta_A|, |\theta_S|\} < \pi,\tag{26}$$

so that the variables within the three spaces are also limited to the ‘machine set’ \mathcal{M} ,

$$\begin{aligned}\mathcal{M}_C &:= \{\mathbf{p} \in \mathbb{R}^2 \mid \{|\bar{\theta}_A(\mathbf{p}, \mathbf{q})|, |\bar{\theta}_S(\mathbf{p}, \mathbf{q})|\} < \pi\}, \\ \mathcal{M}_K &:= \{\{d, \theta_A, \theta_S\} \in \mathbb{R}^3 \mid \{d = \bar{d}(\mathbf{p}, \mathbf{q}), \theta_A = \bar{\theta}_A(\mathbf{p}, \mathbf{q}), \theta_S = \bar{\theta}_S(\mathbf{p}, \mathbf{q})\}, \mathbf{p} \in \mathcal{M}_C\}, \\ \mathcal{M}_P &:= \{\{X_l, Y_l\} \in \mathbb{R}^2 \mid \{X_l = \bar{X}_l(\mathbf{p}, \mathbf{q}), Y_l = \bar{Y}_l(\mathbf{p}, \mathbf{q})\}, \mathbf{p} \in \mathcal{M}_C\}.\end{aligned}\tag{27}$$

The intersection of the inextensibility \mathcal{I} and machine \mathcal{M} sets provides the ‘elastica machine set’ \mathcal{E} , defining the configurations that can be attained by the designed *elastica catastrophe machine*,

$$\mathcal{E}_J := \mathcal{M}_J \cap \mathcal{I}_J, \quad J = C, K, P.\tag{28}$$

The two single-valued functions $\theta_S^{sb(+)}(d, \theta_A)$ and $\theta_S^{sb(-)}(d, \theta_A)$, eqn (15), introduced in the previous section as the collection of critical snap-back (type 1 [8]) conditions for positive and negative sign of ends’ curvature configurations, define respectively the ‘snap-back subsets’ $\mathcal{S}_K^{(+)}$ and $\mathcal{S}_K^{(-)}$ within the $d - \theta_A - \theta_S$ space

$$\begin{aligned}\mathcal{S}_K^{(+)} &:= \left\{ \{d, \theta_A, \theta_S\} \in \mathcal{I}_K \mid \theta_S = \theta_S^{sb(+)}(d, \theta_A) \right\}, \\ \mathcal{S}_K^{(-)} &:= \left\{ \{d, \theta_A, \theta_S\} \in \mathcal{I}_K \mid \theta_S = \theta_S^{sb(-)}(d, \theta_A) \right\}.\end{aligned}\tag{29}$$

The union of the two ‘snap-back subsets’ $\mathcal{S}_K^{(+)}$ and $\mathcal{S}_K^{(-)}$ provides the ‘snap-back set’ \mathcal{S}_K

$$\mathcal{S}_K = \mathcal{S}_K^{(+)} \cup \mathcal{S}_K^{(-)},\tag{30}$$

splitting the $d - \theta_A - \theta_S$ space into two regions, the ‘bistable set’ \mathcal{B}_K collecting kinematical quantities for which two stable solutions exist

$$\mathcal{B}_K := \left\{ \{d, \theta_A, \theta_S\} \in \mathcal{I}_K \mid S_K(d, \theta_A, \theta_S) < 0 \right\},\tag{31}$$

and the ‘monostable set’ \mathcal{U}_K collecting kinematical quantities for which only one stable solution exists

$$\mathcal{U}_K := \left\{ \{d, \theta_A, \theta_S\} \in \mathcal{I}_K \mid S_K(d, \theta_A, \theta_S) > 0 \right\}.\tag{32}$$

⁶The considered limitation for the values of the angles θ_A and θ_S also provides that the machine set does not display type 2 snapping mechanisms [8].

The snap-back set \mathcal{S}_K is independent from the design parameters and has only a representation within the primary kinematical space. Its intersection with the ‘elastica machine set’ \mathcal{E}_K provides the critical kinematical quantities d^c , θ_A^c , and θ_S^c associated with the designed elastica machine and collected in the ‘catastrophe set’⁷ \mathcal{C}_K

$$\mathcal{C}_K := \mathcal{S}_K \cap \mathcal{E}_K = \left\{ \{d^c, \theta_A^c, \theta_S^c\} \in \mathcal{I}_K \mid S_K(d^c = \bar{d}(\mathbf{p}, \mathbf{q}), \theta_A^c = \bar{\theta}_A(\mathbf{p}, \mathbf{q}), \theta_S^c = \bar{\theta}_S(\mathbf{p}, \mathbf{q})) = 0 \right\}. \quad (33)$$

Considering eqns (21) and (??), the ‘catastrophe set’ (or, equivalently, the *catastrophe locus*) \mathcal{C}_K can be also projected within the control and physical⁸ planes

$$\mathcal{C}_C := \{\mathbf{p}^c \in \mathcal{I}_C \mid \mathbf{p}^c = \hat{\mathbf{p}}(\theta_A^c, \theta_S^c)\}, \quad \mathcal{C}_P := \{\{X_l^c, Y_l^c\} \in \mathcal{I}_P \mid X_l = \bar{X}_l(\mathbf{p}^c, \mathbf{q}), Y_l = \bar{Y}_l(\mathbf{p}^c, \mathbf{q})\}. \quad (35)$$

Similarly to the ‘snap-back set’ \mathcal{S}_K , the ‘catastrophe sets’ \mathcal{C}_J are given by the union of the two ‘catastrophe subsets’ $\mathcal{C}_J^{(+)}$ and $\mathcal{C}_J^{(-)}$ ($J = C, K, P$), being the sign referred to that of the symmetric angle/ends curvature for which the equilibrium configuration snaps. Due to the nonlinearities involved, the catastrophe sets can be evaluated only numerically. The algorithm used for the numerical evaluation of the catastrophe set is presented in Section ?? of the Supplementary Material.

3.2 ‘Effectiveness’ of the *elastica catastrophe machine*

Following the principles of the classical catastrophe machine, the ‘effective’ *elastica catastrophe machine* should repetitively display snapping mechanisms along specific equilibrium paths. This property corresponds to the *hysteretic* behaviour typical of nonlinear elastic structures characterized by cusp catastrophes when subject to cyclic variations in their control parameters [25]. Therefore, the design of an ‘effective’ *elastica catastrophe machine* is guided by tuning the design parameters \mathbf{q} towards the morphogenesis of an ‘effective’ catastrophe set \mathcal{C}_P displaying hysteresis. In particular, this set defines a closed curve in the physical plane which is composed of both the ‘catastrophe subsets’ $\mathcal{C}_P^{(+)}$ and $\mathcal{C}_P^{(-)}$ joined together, allowing snapping for both signs of symmetric angle/ends curvature.

The hysteretic (non-hysteretic) behaviour associated to the ‘effectiveness’ (‘non-effectiveness’) of the catastrophe locus is sketched in the upper (lower) part of in Fig. 4 for a cyclic variation in the control parameters.

⁷It is worth mentioning that the present nomenclature differs from that used by some authors [7, 17] defining the projection \mathcal{C}_C of the catastrophe set in the control (force) plane as bifurcation set and the snap-back set \mathcal{S}_K as catastrophe set.

⁸It is noted that the ‘catastrophe set’ \mathcal{C}_P is a curve within the physical plane $X_l - Y_l$, obtained as the projection of the ‘catastrophe set’ \mathcal{C}_P^{3D} collecting the critical rotation angle Θ_l^c as third physical coordinate

$$\mathcal{C}_P^{3D} := \{\{X_l^c, Y_l^c, \Theta_l^c\} \in \mathcal{I}_P \mid X_l = \bar{X}_l(\mathbf{p}^c, \mathbf{q}), Y_l = \bar{Y}_l(\mathbf{p}^c, \mathbf{q}), \Theta_l = \bar{\Theta}_l(\mathbf{p}^c, \mathbf{q})\}. \quad (34)$$

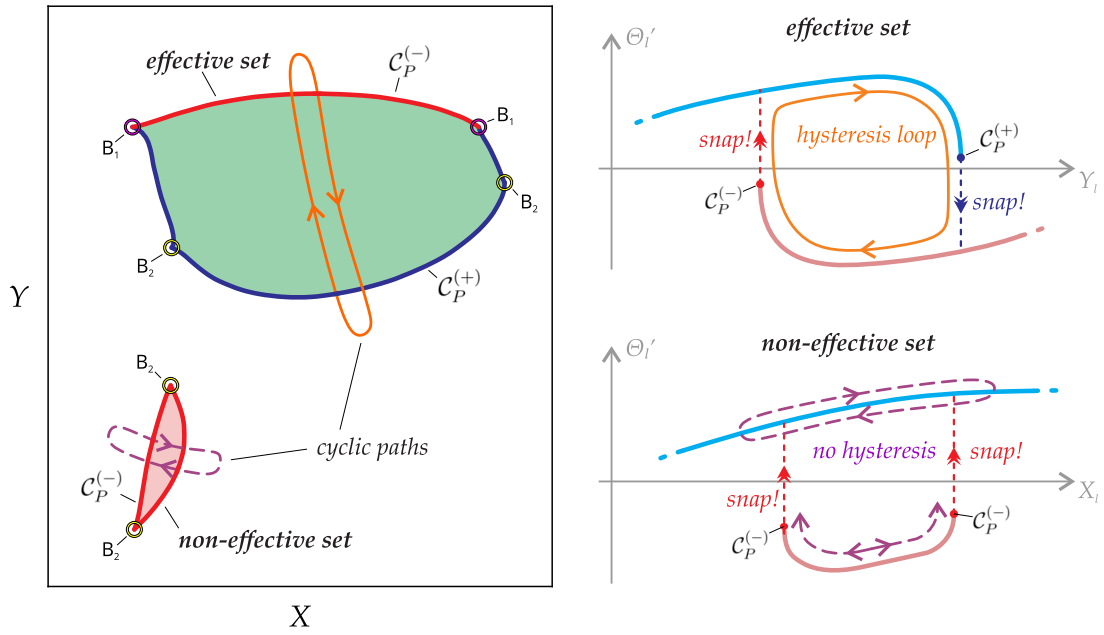


Figure 4: (Left) Sketch of effective and non-effective catastrophe sets within the physical plane, the former composed of the two subsets $\mathcal{C}_P^{(+)}$ (blue curve) and $\mathcal{C}_P^{(-)}$ (red curve) while the latter of a unique closed subset $\mathcal{C}_P^{(-)}$ (red closed curve). Cyclic paths crossing the two sets are drawn as orange and purple closed loops, respectively. Green areas represent the set of coordinates $\{X_l, Y_l\}$ of the rod's end corresponding to bistability of the equilibrium. Sharp corner points B_1 (magenta) and B_2 (yellow) denote supercritical and subcritical bifurcations for the elastica with controlled ends, respectively. (Right) Sketch of the structural response in terms of the end's curvature Θ_l' versus the evolution of the end's coordinate X_l (Y_l) along the orange/continuous (purple/dashed) cyclic path and providing hysteretic (non-hysteretic) behaviour.

The points B_1 (magenta in Fig. 4, left) common to both $\mathcal{C}_P^{(+)}$ and $\mathcal{C}_P^{(-)}$ subsets are present only for effective sets and always correspond to supercritical pitchfork bifurcations as the limit case displaying a non-snapping elastica [8]. Contrarily, the sharp corner points B_2 (yellow in Fig. 4, left) within the subsets $\mathcal{C}_P^{(-)}$ or $\mathcal{C}_P^{(+)}$ are associated with subcritical pitchfork bifurcations displaying high-energy release for the snapping elastica.

Because of its generality, the present theoretical framework can be exploited to design a specific *elastica catastrophe machine* by particularizing the kinematic relations $X_l(\mathbf{p}, \mathbf{q})$, $Y_l(\mathbf{p}, \mathbf{q})$, and $\Theta_l(\mathbf{p}, \mathbf{q})$. Within the infinite set of possible *elastica catastrophe machines*, as evidence of feasibility, two specific families are proposed and investigated in the next section, showing that catastrophe locus can be attained with peculiar properties by tuning the design parameters vector \mathbf{q} . More specifically, the catastrophe locus \mathcal{C}_P of the *elastica catastrophe machine* might exhibit a number of bifurcation points not necessarily equal to four. Indeed, such multiplicity can vary here because coincident with the number, variable through the design parameters, of intersections of the elastica machine set \mathcal{E}_K (which is in general not a plane) with the snap-back set \mathcal{S}_K with $\theta_S = 0$ (points B_1) or $\theta_A = 0$ (points B_2). Even more unusual, the catastrophe locus \mathcal{C}_P may substantially vary its non-convexity, differently from the classical machines. This property is fundamental for crossing bifurcation points at high-energy release. Indeed, convexity facilitates reaching bifurcation points, otherwise confined within acute angles in the classical machines. Because an analytical proof is awkward, with the purpose to evaluate the convex

property of the catastrophe locus \mathcal{C}_P , the convexity measure $C(\mathcal{C}_P)$ is introduced [41]

$$C(\mathcal{C}_P) = \frac{\text{Area}(\mathcal{C}_P)}{\text{Area}(\mathbf{CH}(\mathcal{C}_P))}. \quad (36)$$

In eqn. (36) $\mathbf{CH}(\mathcal{C}_P)$ is the *convex hull* of \mathcal{C}_P , namely the smallest convex set including the shape of the catastrophe locus. The convexity measure C ranges between 0 and 1, being equal to 1 if and only if the planar shape is convex.

4 Two families of *elastica catastrophe machines*

With the purpose to explicitly evaluate catastrophe loci generated by *elastica catastrophe machines*, the two families ECM-I (Fig. 5, left) and ECM-II (Fig. 5, right) are considered and investigated by means of the general theoretical framework presented in the previous section. The elastica's end $s = l$ is considered attached to an external rigid bar, which configuration is defined by the two control parameters p_1 and p_2 . In both ECM-I and ECM-II the control parameter p_2 is taken coincident with the rigid bar rotation, so that, introducing the design angle parameter v between the rigid bar and the elastica end tangent, the rotation Θ_l imposed at the final curvilinear coordinate is given by

$$\Theta_l(\mathbf{p}, \mathbf{q}) = p_2 + v. \quad (37)$$

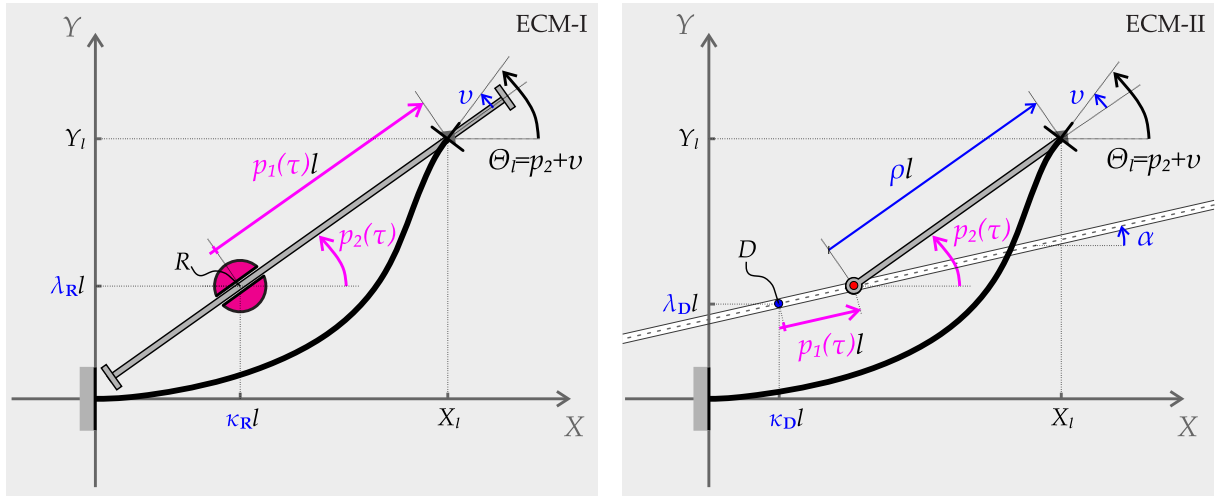


Figure 5: The two proposed families of *elastica catastrophe machine*: ECM-I (left) and ECM-II (right). An inextensible elastic rod of length l has an end with a fixed position and rotation. The kinematics of the elastic rod, considered within the plane $X - Y$, is ruled by the configuration of an external rigid bar defined through two control parameters p_1 and p_2 . The design parameter vectors $\mathbf{q}^I = \{\kappa_R, \lambda_R, v\}$ and $\mathbf{q}^{II} = \{\kappa_D, \lambda_D, \alpha, \rho, v\}$ define respectively a family of *elastica catastrophe machines* ECM-I and ECM-II.

For each one of the two proposed families, the dependence on the control parameters is specified for the physical coordinates $X_l(\mathbf{p}, \mathbf{q})$ and $Y_l(\mathbf{p}, \mathbf{q})$. Therefore, the respective inextensibility and machine sets, introduced in the previous Section with a general perspective, can be explicitly identified. Finally, the shape change of the corresponding catastrophe set and the achievement of ‘effective’ catastrophe sets are disclosed with varying the design parameters vector \mathbf{q} .

4.1 The *elastica catastrophe machine* ECM-I

In the first family of catastrophe machine (Fig. 5, left), the external rigid bar is constrained by a sliding sleeve, centered at the fixed point $R = (\kappa_R l; \lambda_R l)$ and whose inclination with respect to the X -axis corresponds to the control parameter p_2 . By sliding the rigid bar, the distance $p_1 l$ between the elastica end $s = l$ and the sliding sleeve rotation center is ruled by the control parameter p_1 , so that the coordinates of the elastica's end are

$$\bar{X}_l(\mathbf{p}, \mathbf{q}^I) = (\kappa_R + p_1 \cos p_2) l, \quad \bar{Y}_l(\mathbf{p}, \mathbf{q}^I) = (\lambda_R + p_1 \sin p_2) l, \quad (38)$$

with p_1 restricted to positive values ($p_1 > 0$)⁹ and the control parameters vector has length $N = 3$ and is given by

$$\mathbf{q}^I = \{\kappa_R, \lambda_R, v\}. \quad (39)$$

The different relations connecting the configuration representation through control parameters, primary kinematical quantities and physical coordinates can be derived from the explicit kinematical rules (37) and (38). These are reported in the Supplementary Material (Section ??).

The ‘elastica machine set’ \mathcal{E}_C is defined in the control parameters plane $p_1 - p_2$ as the intersection of the inextensibility set \mathcal{I}_C , provided by the inextensibility condition (2) as

$$\mathcal{I}_C = \{\mathbf{p} : p_1^2 + 2p_1 (\kappa_R \cos p_2 + \lambda_R \sin p_2) + \kappa_R^2 + \lambda_R^2 \leq 1\}, \quad (40)$$

with the set machine domain \mathcal{M}_C , eqn (26), expressed as

$$\mathcal{M}_C = \left\{ \mathbf{p} : \left| \frac{p_2 + v}{2} \right| < \pi, \left| \frac{p_2 + v}{2} - \arctan \left(\frac{\lambda_R + p_1 \sin p_2}{\kappa_R + p_1 \cos p_2} \right) \right| < \pi \right\}. \quad (41)$$

The different sets in the primary kinematical space and in the physical plane can be obtained from the respective projections of \mathcal{I}_C (40) and \mathcal{M}_C (41) by means of equations (??)-(??).

The \mathcal{I} , \mathcal{M} , \mathcal{E} , and \mathcal{C} sets are reported in Fig. 6 for the control parameters $\kappa_R = 0.5$, $v = 0$ and $\lambda_R = \{0.3, 0.35, 0.4\}$. Therefore, the considered ECMs-I differ only in the position of the rigid bar rotation center R , slightly moving up from the first to the third line. In the Figure, three different spaces are depicted: the control plane (left column), the primary kinematical space (central column, also containing the snap-back surface \mathcal{S}_K), and the physical plane (right column). The catastrophe set \mathcal{C}_K is evaluated within the primary kinematical space as the curve defined by the intersection of two surfaces, representing the snap set \mathcal{S}_K and the elastica set \mathcal{E}_K . The obtained catastrophe curve has projections \mathcal{C}_C and \mathcal{C}_P within the control and physical planes as planar curves. The positive and negative sign of ends' curvature related to the configuration at snapping is highlighted along the catastrophe curves \mathcal{C} with blue ($\mathcal{C}^{(+)}$) and red ($\mathcal{C}^{(-)}$) colour, respectively. How the catastrophe set changes with increasing the design parameter λ_R may be appreciated from the figure. In particular, the sets of coordinates corresponding to two stable equilibrium configurations are given by the union of one ($\lambda_R = 0.3$), two ($\lambda_R = 0.35$), and three ($\lambda_R = 0.4$) simply connected domains in the physical plane. However, for each of the three cases, only one of these simply connected domains

⁹ It is noted that the catastrophe sets related to negative values (disregarded here) of p_1 can be obtained from those restricted to positive values, being the configuration corresponding to a control vector $\mathbf{p} = \{p_1^b, p_2^b\}$ and a design vector $\mathbf{q}^I = \{\kappa_R^b, \lambda_R^b, v^b\}$ the same of that corresponding to $\mathbf{p} = \{-p_1^b, p_2^b + \pi\}$ and $\mathbf{q}^I = \{\kappa_R^b, \lambda_R^b, v^b - \pi\}$.

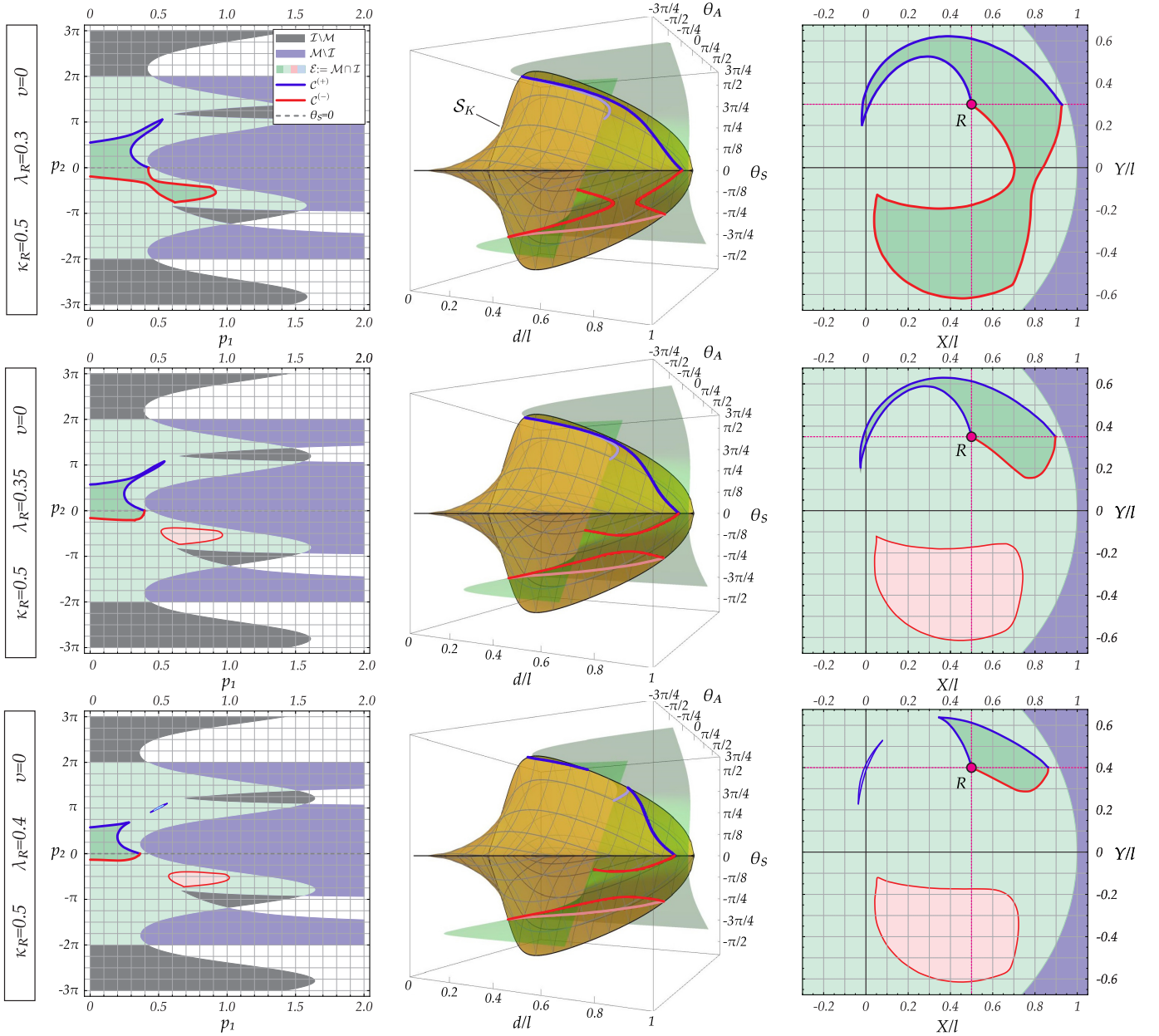


Figure 6: Inextensibility \mathcal{I} , machine \mathcal{M} , elastica \mathcal{E} , and catastrophe \mathcal{C} sets within the three different spaces (from the left to right: control plane, primary kinematical space, physical plane) for three ECMS-I with $\kappa_R = 0.5$, $\nu = 0$ and $\lambda_R = \{0.3, 0.35, 0.4\}$ increasing from the first to the third line. The yellow surface appearing in the primary kinematical space $\{d/l, \theta_A, \theta_S\}$ is the snap-back set \mathcal{S}_K . The portions $\mathcal{C}^{(+)}/\mathcal{C}^{(-)}$ of the ‘catastrophe sets’ are reported as blue/red lines. The effective ‘catastrophe sets’ are reported as thick lines and are those defined by the union of $\mathcal{C}^{(+)}$ with $\mathcal{C}^{(-)}$ (where the superscript is related to the sign of the ends’ curvature of the snapping configuration). The shifting of the rotation centre R parallel to the Y -axis provides a change of the catastrophe locus, with the realization of possible non-effective sets (closed thin lines drawn with only one colour).

(drawn as a thick line) provides hysteresis when crossed during a cyclic path. When existing ($\lambda_R = \{0.35, 0.4\}$), the other simply connected domains have boundary (drawn with thin line) for which snapping occurs only for a positive *or* for a negative sign of the ends' curvature, so that *no more than one* snap (and therefore *no hysteresis*) can be related to these during a cyclic path. The existence and properties of these simply connected domains are strictly dependent on the selected design vector. With this regard, considering¹⁰ only non-negative values of λ_R and $v \in [0, 2\pi)$ and restricting the attention to the physical plane representation, the influence of the design parameters is shown through the following effective and non-effective catastrophe sets:

- for $\kappa_R = 0.5$, $v = \{0, 1\}\pi$, and $\lambda_R = \{0.1, 0.2, 0.3, 0.35, 0.4, 0.5, 0.6, 0.7\}$ in Fig. 7, showing that the *elastica catastrophe machine* is non-effective for both the considered values of v when $\lambda_R = 0.7$, while effective in the remaining cases;
- for $\kappa_R = \{0.25, 0.5, 0.75, 1\}$, $v = \{0, 1/4, 1/2, 3/4, 1, 5/4, 3/2, 7/4\}\pi$, and $\lambda_R = 0$ in Fig. 8, showing that the *elastica catastrophe machine* is non-effective for $\kappa_R = 1$ when $v = \{0, 1/4, 1/2, 3/2, 7/4\}\pi$, while effective in the remaining cases.

Dramatic changes in the projection of the catastrophe set within the physical plane can be observed from these figures, as the result of changing the design parameter vectors \mathbf{q} . In particular, a loss of symmetry in the catastrophe locus occurs when $v \neq \{0, \pi\}$ or $\lambda_R \neq 0$. Furthermore, the catastrophe loci that may be generated by ECM-I encompass a large variety of shapes, very different from those related to the classical catastrophe machines. In particular, the following new features of the catastrophe sets are found:

- *Variable number of bifurcation points.* The effective catastrophe loci, reported for different values of \mathbf{q} in Figs. 7 and 8, display a variable number of bifurcation points depending on the number of intersections of \mathcal{E}_K with \mathcal{S}_K for $\theta_S = 0$ and $\theta_A = 0$. In Fig. 7, the reported effective sets have two (e.g. second row, first column, $v = 0$) or four bifurcation points (e.g. first row, second column, $v = 0$). In Fig. 8, the number of bifurcation points can be equal to one (e.g. first row, first column, $v = \pi$), two (e.g. second row, second column, $v = \pi/4$), three (first row, first column, $v = 0$) or four (second row, first column, $v = \pi/4$);
- *Convex measure of the catastrophe locus \mathcal{C}_P .* In Fig. 8, the catastrophe sets for $\{v = \pi, \kappa_R = 0.25\}$ (first row, first column) and for $\{v = 0, \kappa_R = 0.75\}$ (first row, third column) have convex measure approaching the unit value, $C \simeq 1$. The catastrophe set for $\{v = \pi, \kappa_R = 0.5\}$ (first row, second column) has $C = 0.9997$ while that for $\{v = \pi, \kappa_R = 0.75\}$ (first row, third column) has $C = 0.998$. Finally, the catastrophe sets for $v = 0$ and $\lambda_R = \{0.3, 0.35, 0.4\}$ shown in Figs. 6 and 7 have $C = \{0.5707, 0.4475, 0.9402\}$.

The recommendations about how to select the initial values of the control parameters $\mathbf{p}(\tau_0)$ to belong to the inextensibility set \mathcal{I}_C are included in Sect. ?? of the Supplementary Material.

¹⁰Symmetry and periodicity properties of expressions (37) and (38) in the design parameters λ_R and v define symmetry properties for the catastrophe sets. More specifically, a change in the sign of both the design parameters λ_R and v provides a mirroring of the catastrophe set (with respect to the X axis within the physical plane and with respect to the p_2 within the control plane) and a change in sign for the related curvature displaying snapping. An increase of $2k\pi$ ($k \in \mathbb{Z}$) in v provides a shifting of $-2k\pi$ of the catastrophe set with respect to the p_2 axis within the control plane and no change within the physical plane.

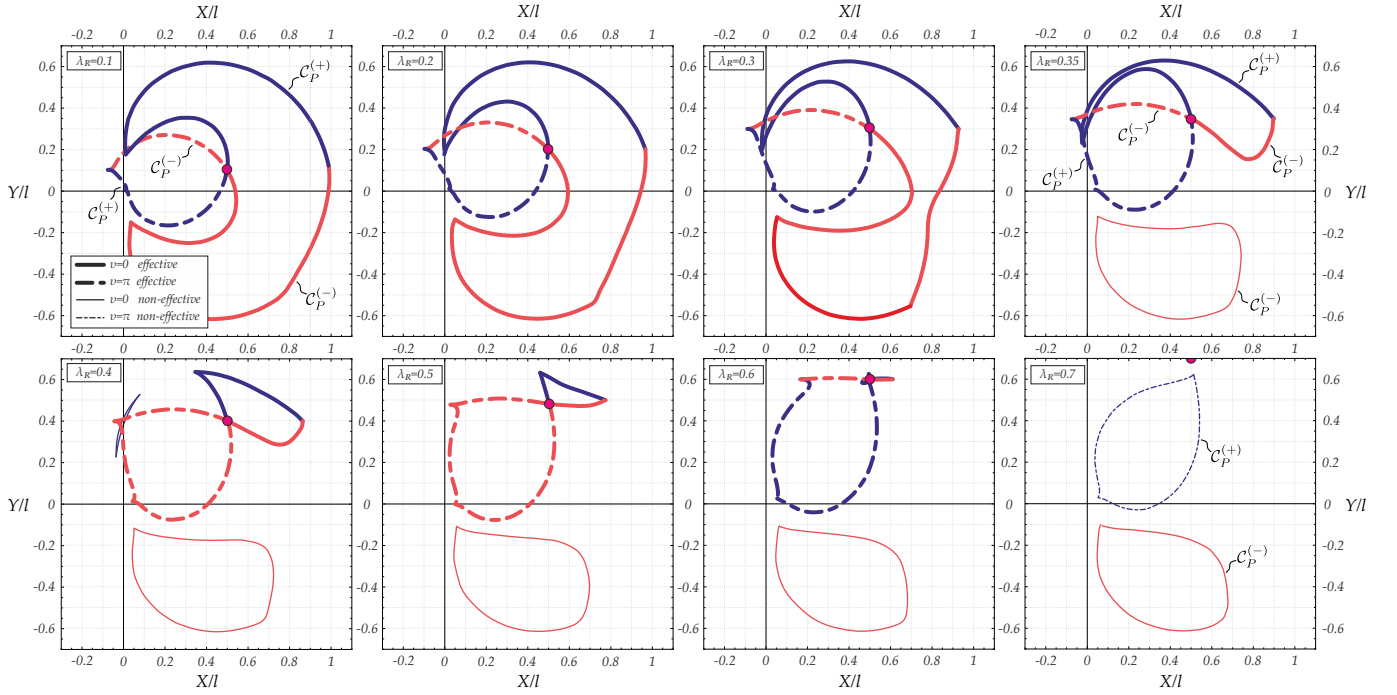


Figure 7: Catastrophe loci in the physical plane $X - Y$ for ECM-I with $\kappa_R = 0.5$, $\lambda_R = \{0.1, 0.2, 0.3, 0.35, 0.4, 0.5, 0.6, 0.7\}$, and $v = \{0, 1\}\pi$. The red spots identify the position rotation center R of the rigid bar. Effectiveness and non-effectiveness of the catastrophe loci is distinguished through thick and thin coloured lines, respectively.

Some considerations drawn for ECM-I under the two special conditions for the position center R are respectively reported in Sects. ?? and ??) of the Supplementary Material. Similarly to the classical Zeeman machine, all the sharp corner points, when not coincident with the rotation centre R , correspond to pitchfork bifurcations.

4.2 The *elastica catastrophe machine* ECM-II

In the catastrophe machine ECM-II (Fig. 5, right) the rigid bar of fixed length ρl can rotate and has one end constrained to slide along a straight line, inclined at an angle α with respect to the X -axis. The center of rotation of the rigid bar is at a controlled distance $p_1 l$ from a fixed point D , of coordinates $\{X_D, Y_D\} = \{\kappa_D, \lambda_D\}l$, located on the straight line. By controlling the inclination p_2 and the distance $p_1 l$ of the movable rotation center of coordinates $\{\kappa_D + p_1 \cos \alpha, \lambda_D + p_1 \sin \alpha\}l$ from the reference point D , the elastica end $s = l$ has coordinates

$$\bar{X}_l(\mathbf{p}, \mathbf{q}^{II}) = (\kappa_D + p_1 \cos \alpha + \rho \cos p_2) l, \quad \bar{Y}_l(\mathbf{p}, \mathbf{q}^{II}) = (\lambda_D + p_1 \sin \alpha + \rho \sin p_2) l, \quad (42)$$

while the design parameters vector (of length $N = 5$) for ECM-II is

$$\mathbf{q}^{II} = \{\kappa_D, \lambda_D, \alpha, \rho, v\}. \quad (43)$$

The equations relating the control parameters, the primary kinematical quantities and the physical coordinates are obtained through the equations (37) and (42) and reported in the Supplementary Material (Section ??).

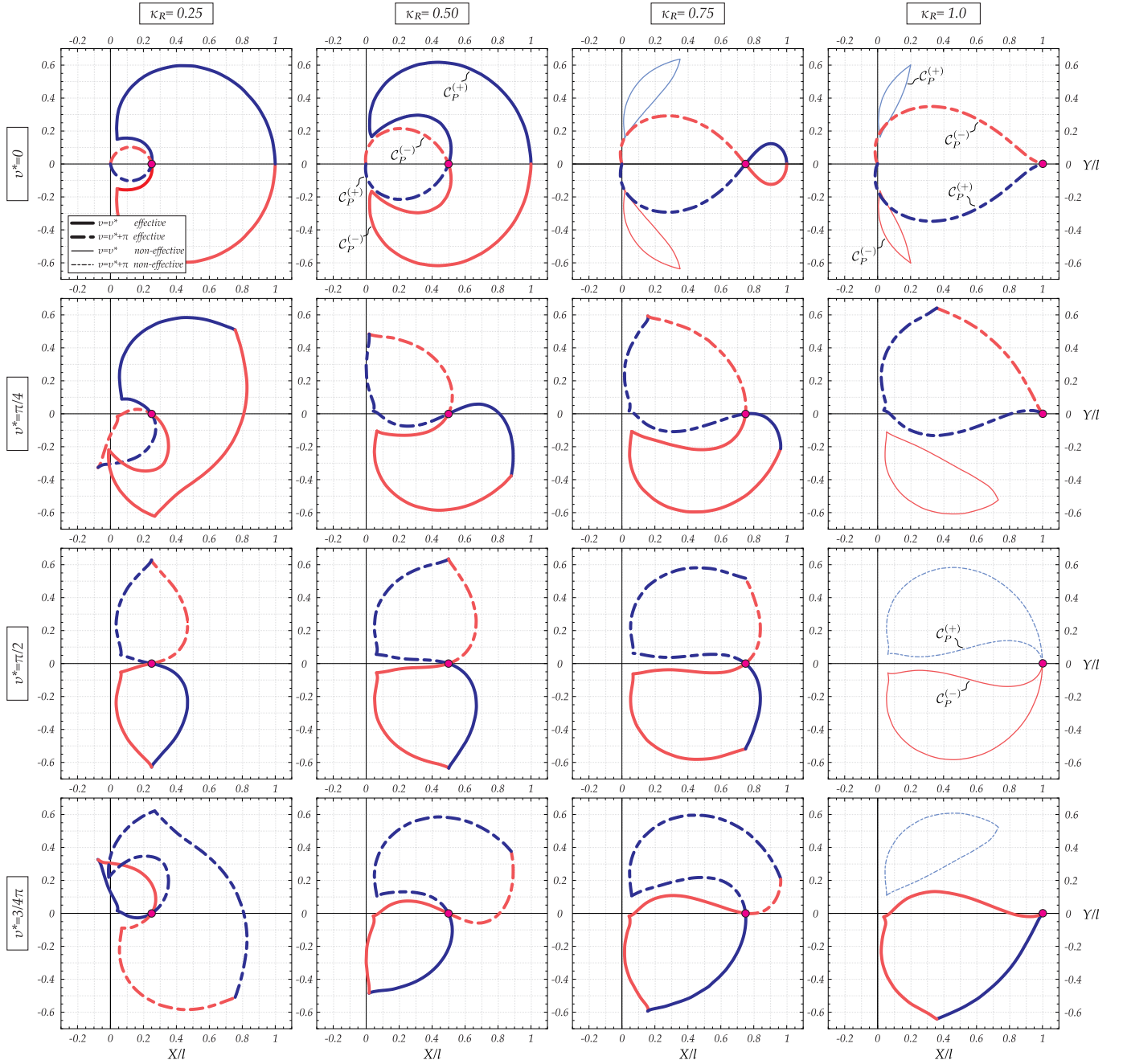


Figure 8: As for Fig. 7, but for $\lambda_R = 0$, $\kappa_R = \{0.25, 0.5, 0.75, 1\}$ and $v = \{0, 1/4, 1/2, 3/4, 1, 5/4, 3/2, 7/4\}\pi$. The parameter v^* is introduced to represent the two cases $v = v^*$ and $v = v^* + \pi$ in the same plot. The position rotation center R of the rigid bar is identified as red spots.

The control parameters vector \mathbf{p} for ECM-II is restricted to the set \mathcal{E}_C , given by the intersection of the inextensibility set \mathcal{I}_C ,

$$\mathcal{I}_C = \left\{ \mathbf{p} : p_1^2 + \rho^2 + 2[p_1\rho\cos(\alpha - p_2) + \kappa_D(p_1\cos\alpha + \rho\cos p_2) + \lambda_D(p_1\sin\alpha + \rho\sin p_2)] + \kappa_D^2 + \lambda_D^2 \leq 1 \right\}, \quad (44)$$

with the machine domain \mathcal{M}_C

$$\mathcal{M}_C = \left\{ \mathbf{p} : \left| \frac{p_2 + v}{2} \right| < \pi, \left| \frac{p_2 + v}{2} - \arctan \left(\frac{\lambda_D + p_1 \sin \alpha + \rho \sin p_2}{\kappa_D + p_1 \cos \alpha + \rho \cos p_2} \right) \right| < \pi \right\}. \quad (45)$$

In order to have a non-null elastica machine set \mathcal{E} , the first four design parameters are constrained to satisfy the following inequality

$$|\kappa_D \sin \alpha - \lambda_D \cos \alpha| - \rho < 1. \quad (46)$$

From eqn (42), it may also be noted that two different control parameters vectors \mathbf{p}^b and \mathbf{p}^\sharp provide the same end's coordinates $\{X_l(\mathbf{p}^b, \mathbf{q}) = X_l(\mathbf{p}^\sharp, \mathbf{q}), Y_l(\mathbf{p}^b, \mathbf{q}) = Y_l(\mathbf{p}^\sharp, \mathbf{q})\}$ when

$$p_1^\sharp = p_1^b + 2\rho \cos(p_2^b - \alpha), \quad p_2^\sharp = \pi + 2\alpha - p_2^b. \quad (47)$$

Therefore, in addition to the natural multiplicity due to the angular periodicity in the physical angle Θ_l , the same position X_l, Y_l in the physical plane is associated to two physical angles $\Theta_l(\mathbf{p}^\sharp, \mathbf{q}) \neq \Theta_l(\mathbf{p}^b, \mathbf{q})$ not differing by $2k\pi$ ($k \in \mathbb{Z}$), namely

$$\Theta_l(\mathbf{p}^\sharp, \mathbf{q}) = \pi + 2(\alpha + v) - \Theta_l(\mathbf{p}^b, \mathbf{q}). \quad (48)$$

Due to this additional multiplicity, it is instrumental to analyze the behaviour of ECM-II through the analysis of two machine subtypes, ECM-IIa and ECM-IIb, having the control parameter p_2 (ruling the rigid bar rotation) restricted to specific sets $p_2^{(a)}$ and $p_2^{(b)}$,

$$\begin{aligned} \text{ECM-IIa: } p_2^{(a)} &\in \bigcup_{k \in \mathbb{Z}} \left[-\frac{\pi}{2} + \alpha + 2k\pi, \frac{\pi}{2} + \alpha + 2k\pi \right], \\ \text{ECM-IIb: } p_2^{(b)} &\in \bigcup_{k \in \mathbb{Z}} \left[\frac{\pi}{2} + \alpha + 2k\pi, \frac{3\pi}{2} + \alpha + 2k\pi \right]. \end{aligned} \quad (49)$$

The inextensibility \mathcal{I} , the machine \mathcal{M} , the elastica \mathcal{E} and catastrophe \mathcal{C} sets for ECM-II are shown in Fig. 9 within the control plane (left column), primary kinematical space (central column), and the physical plane (right column) for $\kappa_D = \lambda_D = \alpha = v = 0$ and $\rho = \{0.5, 0.6, 0.65\}$, with increasing values from the upper to the lower line. The portions $\mathcal{C}_P^{(+)} / \mathcal{C}_P^{(-)}$ of catastrophe loci are reported as blue/red lines, continuous for ECM-IIa and dashed for ECM-IIb. In the figure, the blue/red line defines configurations for which elastica with positive/negative ends curvature snaps. The thick line identifies an effective catastrophe locus while a thin line a non-effective one, so that, in Fig. 9, the catastrophe sets of EMC-IIa are all effective while those of ECM-IIb are not. It is evident that for $\rho = \{0.5, 0.6\}$ the catastrophe sets of ECM-IIa and ECM-IIb have in common their end points (also at the boundary of \mathcal{I}/\mathcal{M} in the physical plane) while for $\rho = 0.65$ the two machine subtypes do not share any point with each other.

The catastrophe sets of ECM-IIa and ECM-IIb for $\kappa_D = \lambda_D = \alpha = v = 0$ and $\rho = 0.5$ shown in Fig. 9 (upper part, right) are also reported separately for the two machine subtypes in Fig. 10 (upper part). This latter representation contains also some elasticae, highlighting the two possible equilibrium configurations for a state within the bistable region and the only possible configuration after crossing the catastrophe locus. The catastrophe sets are also reported in the lower part of Fig. 10 for a machine with the same design parameters of that considered in the upper part of Fig. 10 except for the value of v , taken as $v = \pi$ (instead of $v = 0$).

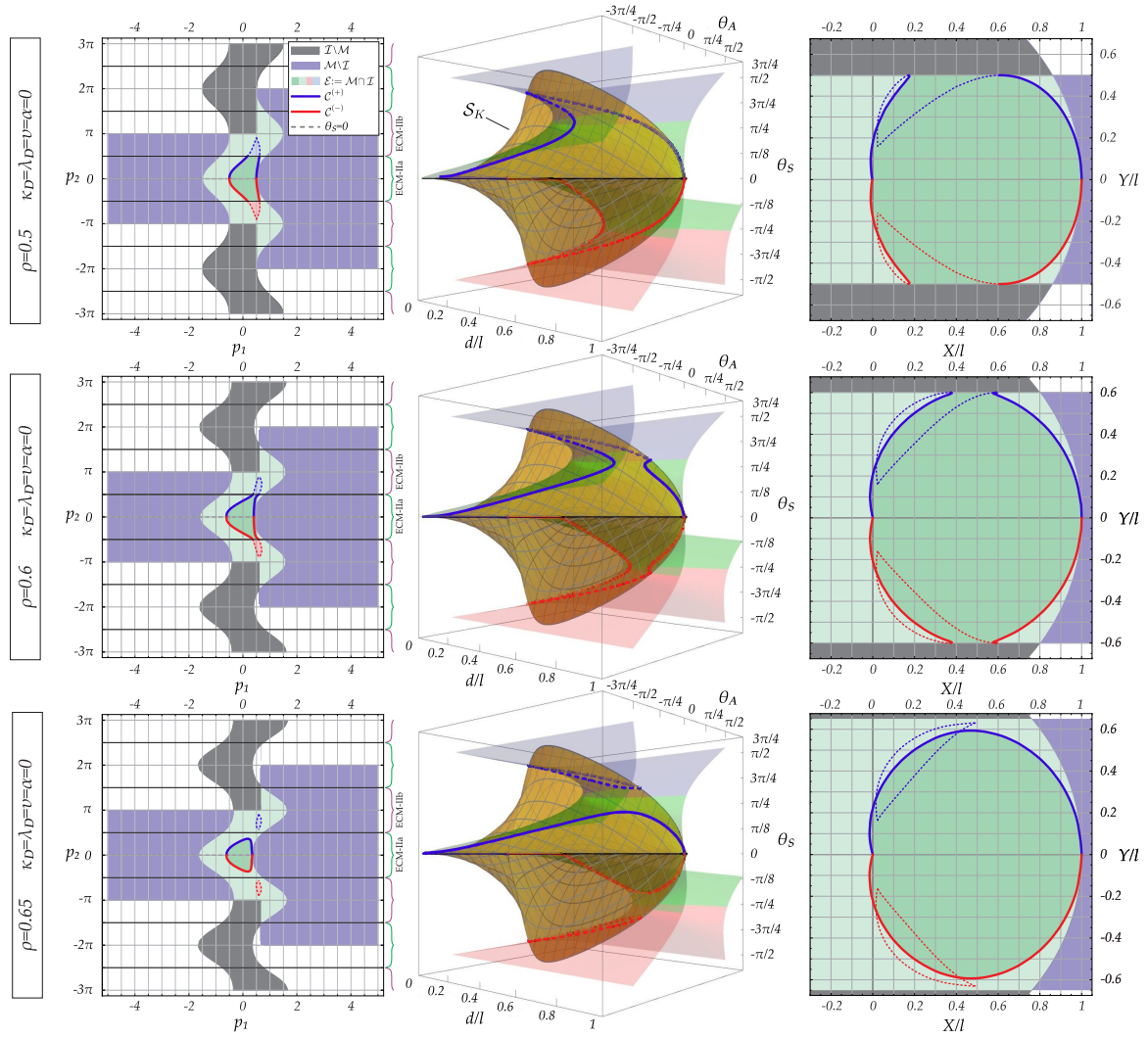


Figure 9: As for Fig. 6, but for three ECMs-II with $\kappa_D = \lambda_D = v = \alpha = 0$ and $\rho = \{0.5, 0.6, 0.65\}$ increasing from the first to the third line. The portions $\mathcal{C}^{(+)}/\mathcal{C}^{(-)}$ of the ‘catastrophe sets’ are reported as blue/red lines, continuous for ECM-IIa and dashed for ECM-IIb. For the reported cases, the effective ‘catastrophe sets’ are related only to ECM-IIa. The increase in the rigid bar parameter length ρ provides a change of the catastrophe locus, as the detachment from the elastica machine set boundary in the case $\rho = 0.65$.

It can be appreciated that for the same design parameters no more than one of the two machine subtypes is effective, namely ECM-IIa with $v = 0$ and ECM-IIb with $v = \pi$. The remaining two machine subtypes are non-effective, but each of them displays a different behaviour. ECM-IIb with $v = 0$ has a non-effective catastrophe set so that only one snap may occur during a continuous evolution while ECM-IIa with $v = \pi$ has no catastrophe locus so that no snap is possible with this machine subtype. Performing a parametric analysis of ECM-II (by varying the design parameters) it can be concluded that a principle of exclusion about the effectiveness for the two subtypes of machine exists, namely, if ECM-IIa (or ECM-IIb) is an effective machine then ECM-IIb (or ECM-IIa) is not. This principle finds also evidence in the Figs. 11-14, referred to different design parameters vectors (restricted to $v \in [0, 2\pi)$ due

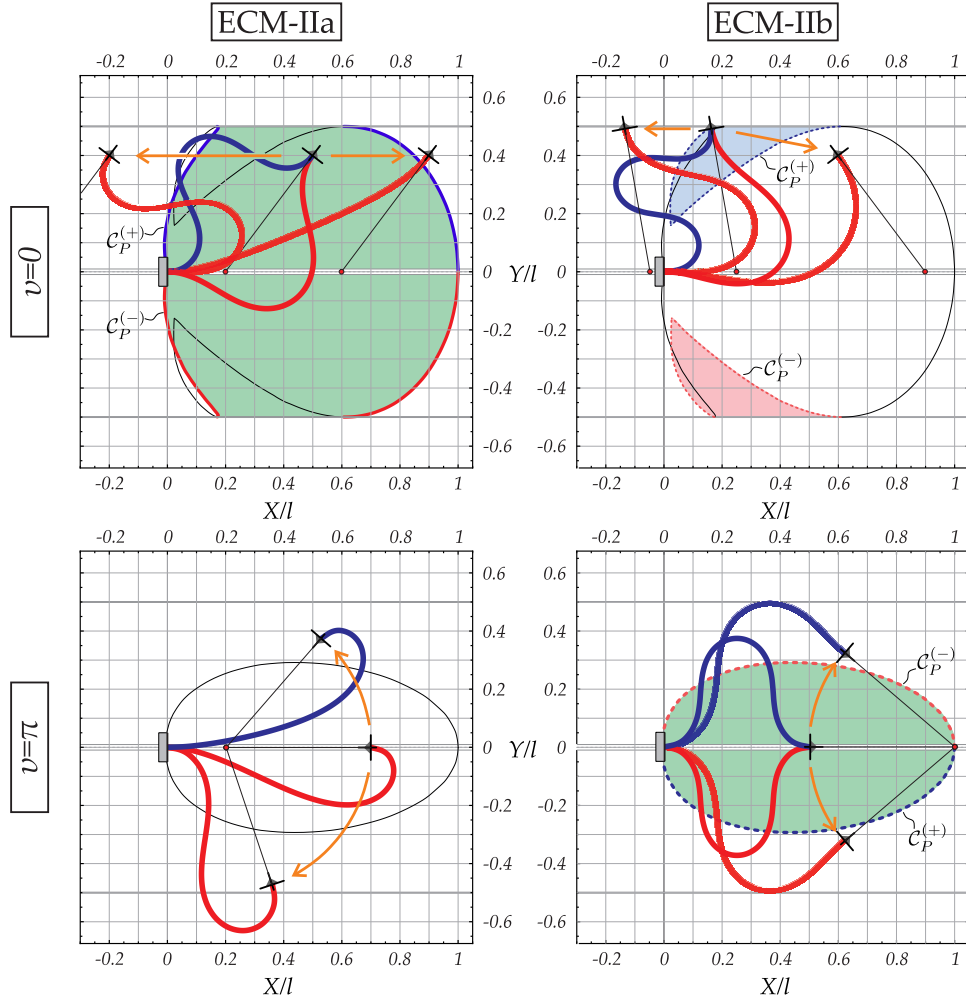


Figure 10: Catastrophe sets of ECM-IIa and ECM-IIb with $\kappa_D = \lambda_D = \alpha = 0$, $\rho = 0.5$, and $v = 0$ (upper part) or $v = \pi$ (lower part). While ECM-IIa is effective for $v = 0$, ECM-IIb is effective for $v = \pi$. Deformed configurations are also displayed for some specific end's position, highlighting equilibrium multiplicity (when existing).

to periodicity) as follows:

- for $\kappa_D = \lambda_D = \alpha = 0$, $\rho = \{0.1, 0.2, 0.3, 0.5, 0.6, 0.7, 0.8, 1\}$ and $v = 0$ in Fig. 11 and for the same values of λ_D , κ_D , α , and ρ but $v = \pi$ in Fig. 12, showing that only ECM-IIa is effective in the former figure while only ECM-IIb is effective in the latter. In particular, ECM-IIa does not display any catastrophe set in all the cases in Fig. 12 (similarly to Fig. 10, bottom left) except when $\rho = 1$;
- for $\kappa_D = \lambda_D = 0$, $\rho = 0.5$, $v = \{0, \pi\}$ and $\alpha = \{0, 1/8, 1/4, 1/2\}\pi$ in Fig. 13, showing that only ECM-IIa is effective for $v = 0$ and $\alpha = \{0, 1/8, 1/4\}\pi$, only ECM-IIb is effective for $v = \pi$ and $\alpha = \{0, 1/8\}\pi$, while no machine subtype is effective in the remaining cases;
- for $\kappa_D = \alpha = 0$, $\rho = 0.5$, $\lambda_D = \{0, 0.2, 0.4, 0.6\}$ and $v = \{0, 1/4, 1/2, 3/4\}\pi$ in Fig. 14, showing that only ECM-IIa is effective for $v = \{0, 1/4\}\pi$ for all the reported values of

λ_D and only ECM-IIb is effective for $v = 3/4\pi$ for all the reported values of λ_D , while no machine subtype is effective in the remaining cases.

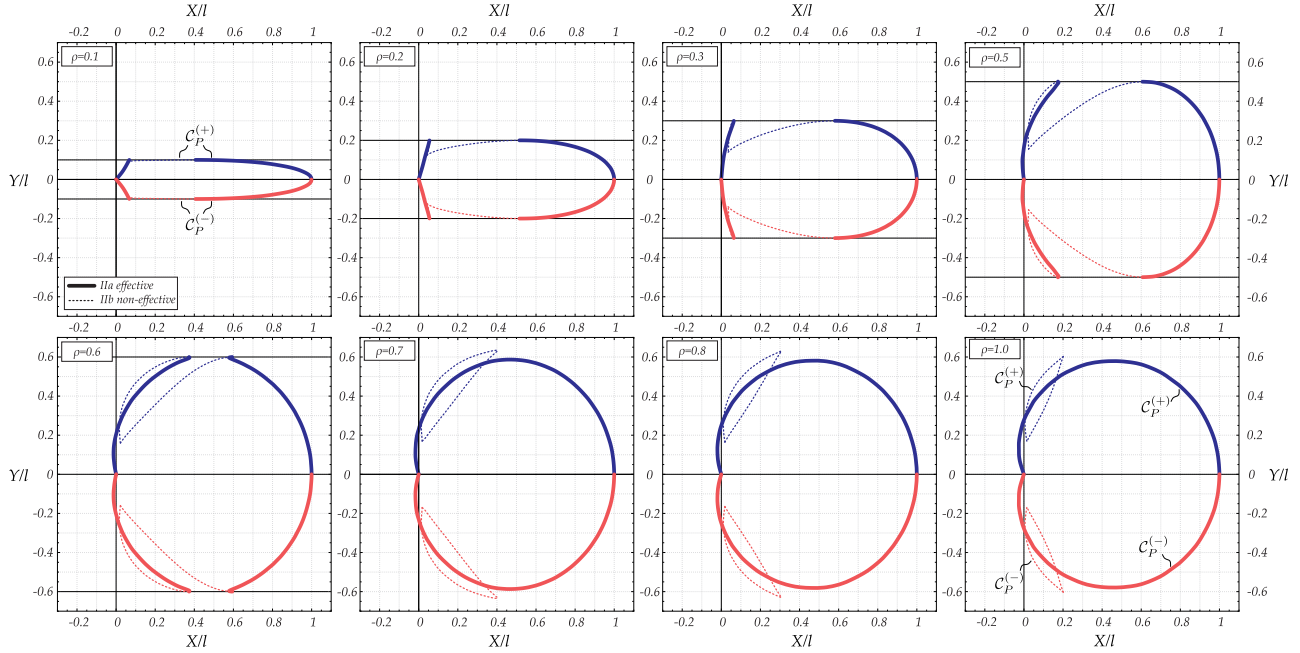


Figure 11: Catastrophe loci in the physical plane $X - Y$ for ECM-II with $\kappa_D = \lambda_D = \alpha = v = 0$ and $\lambda_D = \{0.1, 0.2, 0.3, 0.5, 0.6, 0.7, 0.8, 1\}$. Sets related to ECM-IIa are represented by continuous lines while those related to ECM-IIb by dashed lines. Effectiveness and non-effectiveness of the catastrophe loci is distinguished through thick and thin coloured lines, respectively.

In analogy with the observations for ECM-I machine, the following new features of the catastrophe sets for ECM-II are displayed:

- *Variable number of bifurcation points.* The catastrophe sets in Figs. 11, 12, 13 and 14 exhibit a number of bifurcation points ranging from two to five. For instance, the ECM-IIa machines in Fig. 11 and the ECM-IIb machines in Fig. 12 have a catastrophe set with two bifurcation points on the symmetry axis. Moreover, In Fig. 14, the catastrophe set for the ECM-IIa machine for $v = \pi/4$ and $\lambda_D = 0.2$ (second row and second column) has five bifurcation points.
- *Convex measure of the catastrophe locus C_P .* The catastrophe sets reported in the first row of Fig. 12 have $C \simeq 1$ for $\rho = \{0.1, 0.2, 0.3\}$ (first three columns) and $C = 0.9998$ for $\rho = 0.5$ (fourth column).

The three-dimensional representation in Fig. 15 shows the curvature at the final curvilinear coordinate as a function of the two control parameters for ECM-IIb with $\kappa_D = \lambda_D = \alpha = 0$, $v = \pi$, and $\rho = 0.8$ (corresponding to the setting considered in the third column, second line, of Fig. 12). The same three-dimensional plot is reported on the left and the right under two opposite perspectives. Multiplicity and uniqueness of equilibrium configuration are highlighted for control parameters pairs respectively inside and outside the closed curve defining the catastrophe locus (projection on the $p_1 - p_2$ plane). The jump in the equilibrium

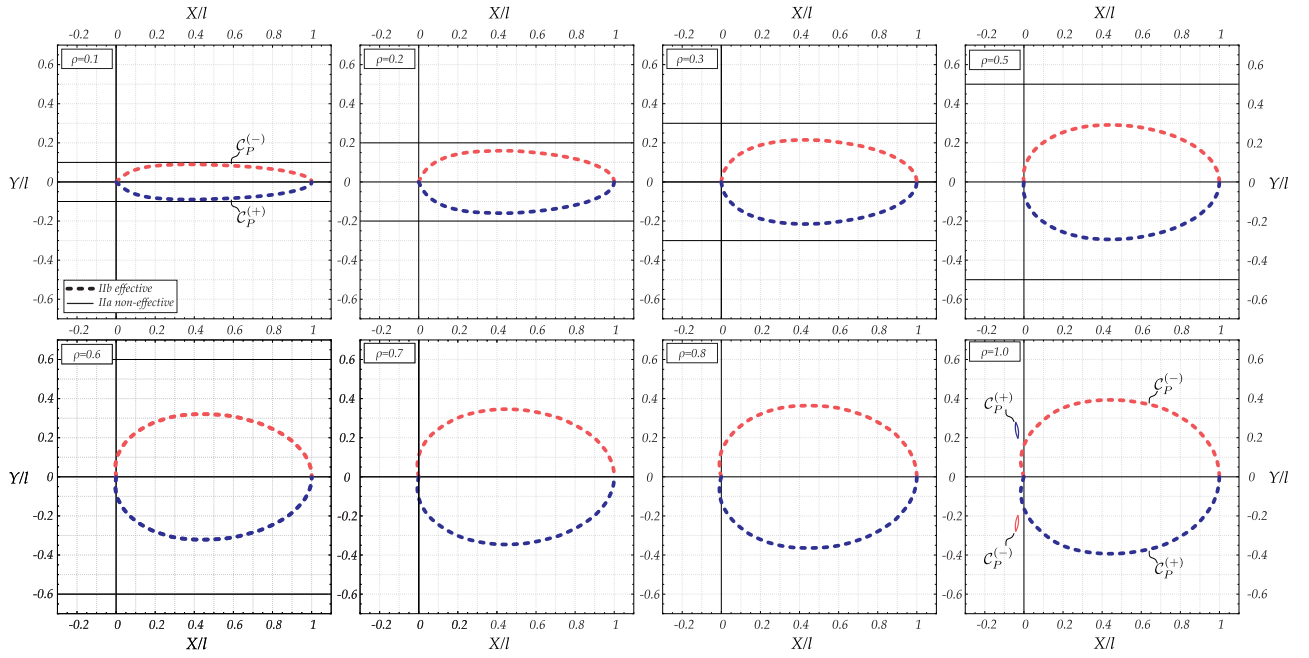


Figure 12: As for Fig. 11, but for $\nu = \pi$.

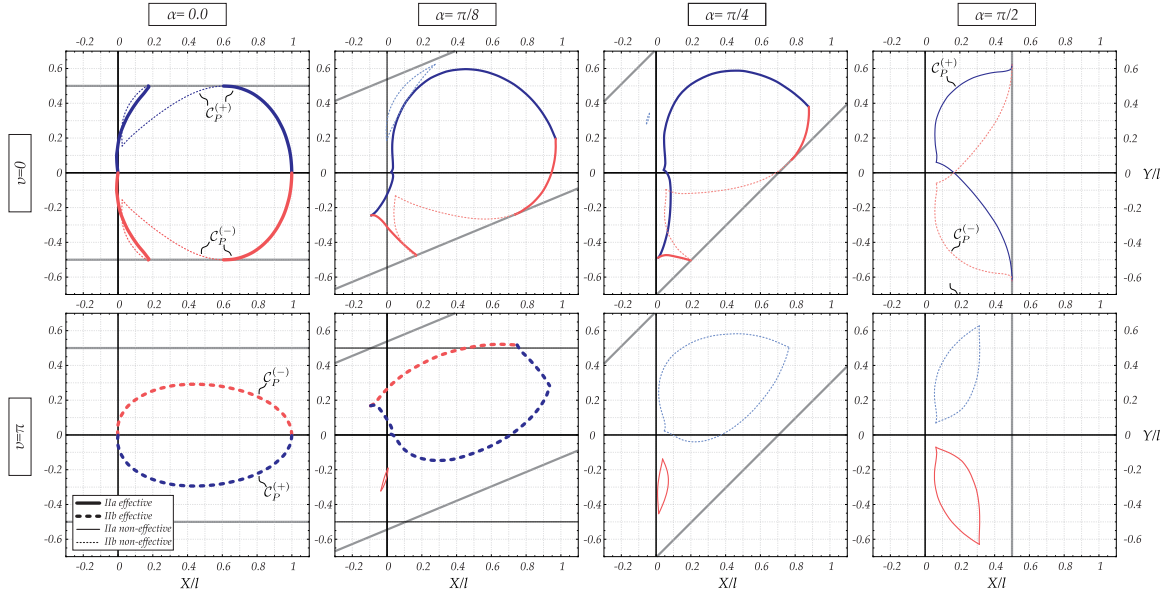


Figure 13: As for Fig. 11, but for $\kappa_D = \lambda_D = 0$, $\rho = 0.5$. A constant value of ν is considered for each line (first line $\nu = 0$, second line $\nu = \pi$) and of α for each column ($\alpha = \{0, 1/8, 1/4, 1/2\}\pi$, increasing from left to right).

configuration, displayed at the catastrophe locus with arrows, implies a change in the curvature sign (for the same value of control parameters).

Finally, the analysis of ECM-II is complemented by a discussion about the special case of the rigid bar with infinitely large length reported in Sect. ?? of the Supplementary Material and the suggestion for the initial values of the control parameters $\mathbf{p}(\tau_0)$ in Sect. ?? of the

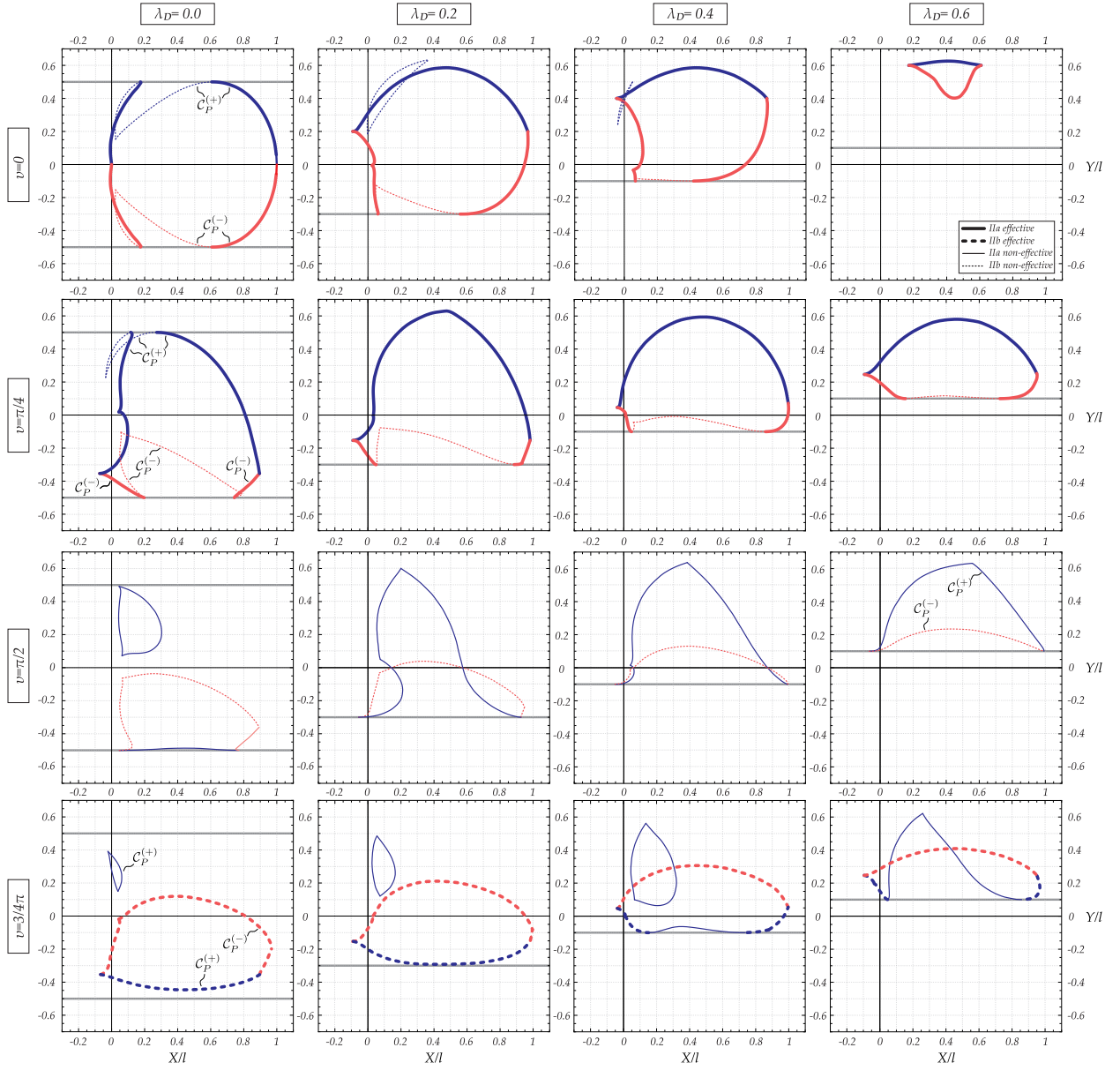


Figure 14: As for Fig. 11, but for $\kappa_D = \alpha = 0$, $\rho = 0.5$. A constant value of v is considered for each line ($v = \{0, 1/4, 1/2, 3/4\}\pi$, increasing from above to bottom) and of λ_D for each column ($\lambda_D = \{0, 0.2, 0.4, 0.6\}$, increasing from left to right).

Supplementary Material.

5 The physical realization of the *elastica catastrophe machine*

A prototype of the *elastica catastrophe machine* was designed and realized at the Instabilities Lab of the University of Trento, Fig. 16. This setup, thought to be as versatile as possible, allowed the experimental investigation of both the two proposed families, ECM-I and ECM-II

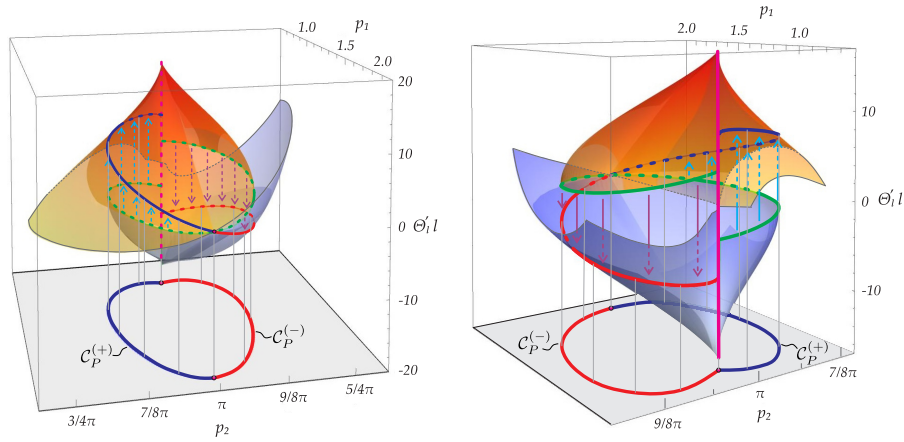


Figure 15: Curvature at the final curvilinear coordinate, $\Theta'_l = \Theta'(s = l)$, (made dimensionless by multiplication with the length l) as a function of the control parameters p_1 and p_2 for ECM-IIb with $\kappa_D = \lambda_D = \alpha = 0$, $v = \pi$, and $\rho = 0.8$ (corresponding to the setting considered in the third column, second line, of Fig. 12). Two opposite views of the three-dimensional plot are reported on the left and the right. Green line highlights critical configurations for which snap occurs toward a configuration laying along the blue and red curve having the same control parameters pair but opposite curvature sign. The projection of $\mathcal{C}^{(+)}$ (blue line) and $\mathcal{C}^{(-)}$ (red line) on the $p_1 - p_2$ plane is also reported as the representation of the catastrophe locus within the control plane.

(a and b). The two clamps, one fixed and the other moving, constraining the ends of the elastic rod are assembled on an HDF (High-density fibreboard) desk. This panel acts as a support for mounting the screen printing of the catastrophe locus, which changes by varying the selected design parameters. More specifically, the clamp constraint at the rod coordinate $s = 0$ is fixed and mounted on a PMMA structure. The constraint at the other end of the rod ($s = l$) is provided by a clamp which may slide along a rotating aluminium hollow bar (10×10 mm cross-section) with its end pinned to and possibly sliding along an aluminium rail (aluminium extrusions bar, 20×20 mm cross-section), fixed on the desk through two clips. Three goniometers are mounted to measure during the experiments (i.) the angle between the desk and the rail (design angle α in ECM-II), (ii.) the angle between the rail and the rotating bar (to be used for imposing the control angle p_2), and (iii.) the angle between the rotating bar and the moving clamp inclination (design angle v).

Each one of the two proposed families can be tested by properly constraining one of the degrees of freedom of the prototype to a fixed value. In particular, ECM-I is attained by fixing the rotating bar end to a specific point R (design parameters κ_R, λ_R) along the fixed rail, while ECM-II by fixing the moving clamp along the rotating bar at a distance ρl from its end and by defining the inclination α and the passing point D (design parameters κ_D, λ_D) for the fixed rail.

Rods of (net) length $l = 40$ cm with different cross-sections and made up of different materials have been tested. In the following, results are shown for two types of rods: a polikristal rod (by Polimark, Young modulus $E = 2750$ MPa, density $\rho = 1250$ kg m $^{-3}$) with a cross section 20×0.8 mm, and a carbon fiber rod (by CreVeR srl, Young modulus $E = 80148$ MPa, density $\rho = 1620$ kg m $^{-3}$) with a cross section 20×0.45 mm.

The ECM prototype was tested as EMC-I, ECM-IIa, and ECM-IIb for different continuous evolutions of the moving clamp position repetitively crossing the catastrophe locus and provid-

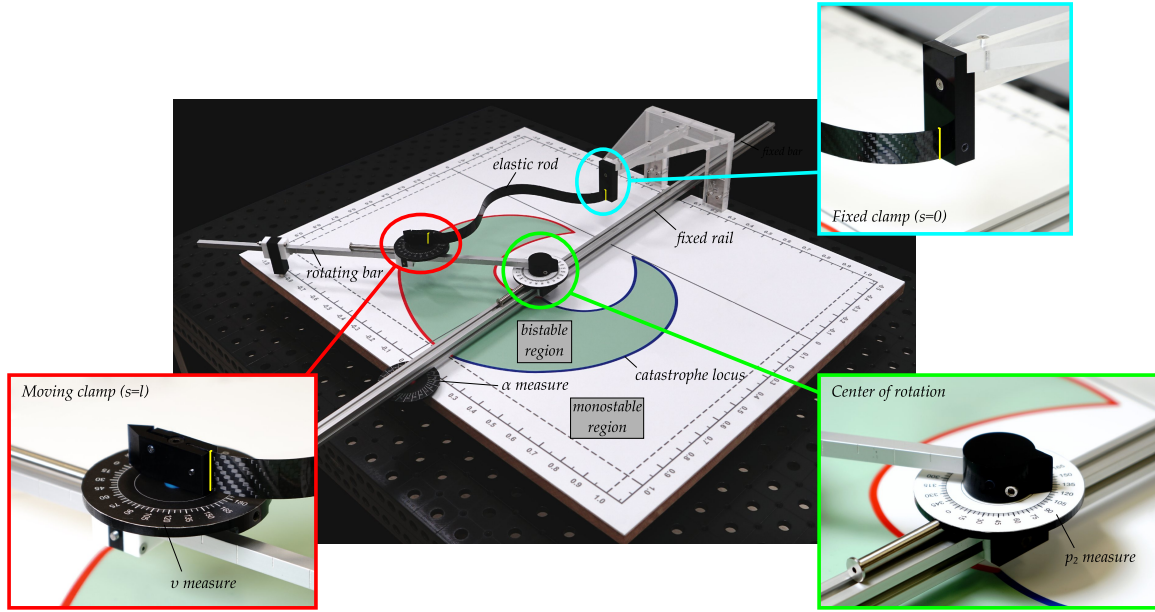


Figure 16: Prototype of the *elastica catastrophe machine*. A (carbon fiber) rod constrained at its two ends by a fixed clamp (inset upper right, cyan) and another clamp (inset lower left, red) which may move along a stiff bar, which, in turn, may rotate about its end pinned and possibly moving along a fixed rail (inset lower right, green). The rail is fixed to the plastic desk through two clips. The angles v and α can be respectively measured from the black goniometers fixed on the movable clamp and the plane, while the angle p_2 can be measured from the white goniometer fixed at the rotation centre of the stiff bar.

ing a sequence of snapping mechanisms. Photos taken at specific stages during the experiments are displayed in Fig. 17. In the figure, all the stable equilibrium configurations are reported at three stages for ECM-I (with $\kappa_R = 0.5$, $\lambda_R = 0.1$, $v = 0$). The three stages are related to the position of the moving clamp, located (a) within the bistable region, (b) on the catastrophe locus, and (c) within the monostable region (from left to right in Fig. 17). The two equilibrium configurations related to each of the two first stages (left and central column) differ in the curvature sign at the clamps and are displayed as the superposition of two photos. The only ‘surviving’ configuration is displayed at stage c (right column), which can be reached through a smooth transition from the adjacent deformed configuration or through snapping from the non-adjacent deformed configuration (characterized by an opposite sign of the curvature at both clamps). The experimental results are reported for a clamp position’s evolution ruled by different variations of the control parameters: (i) variation in both the control parameters p_1 and p_2 (Fig. 17, upper part) and (ii) variation in the control parameter p_1 at fixed value of p_2 (Fig. 17, lower part).

The transition of the deformed configuration during a continuous evolution is highlighted in Figs. 2 (for ECM-I with $\kappa_R = 0.5$, $\lambda_R = 0.1$, $v = 0$). Four snapshots captured during the fast motion at snapping (taken with a high-speed camera *Sony PXW-FS5*, 120 fps) are superimposed in the second column of the figure (the deformed configurations are highlighted with purple dashed lines), where each two consecutive snapshots are referred to a time interval of approximately 0.15 sec. These sequences display the rod motion towards the change of curvature sign at both clamps. Further experiments performed on different ECM are reported in the section ?? of the Supplementary Material.

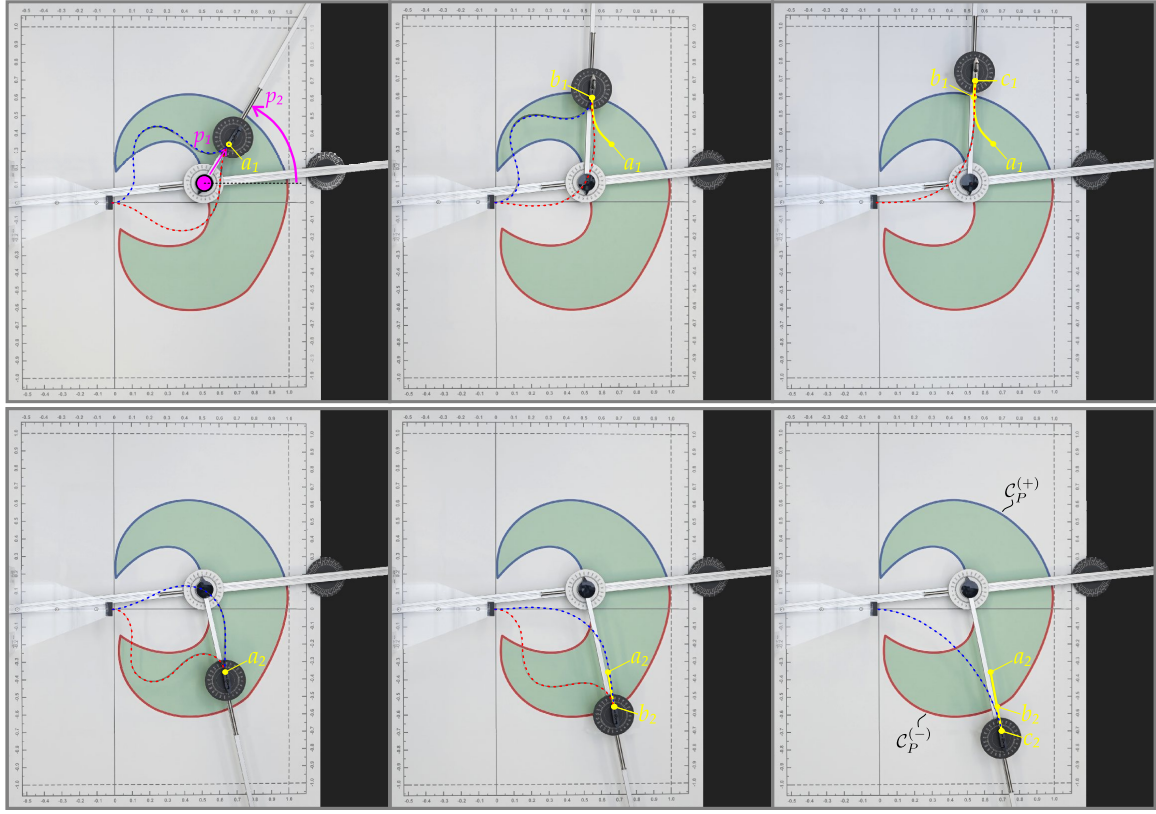


Figure 17: Evolution of the equilibrium configurations for a carbon fiber rod in the ECM-I (with $\kappa_R = 0.5$, $\lambda_R = 0.1$, $v = 0$) with varying the position of the moving clamp: within the bistable (green background) region (stage *a*, left column), on the catastrophe locus (stage *b*, central column), and within the monostable region (stage *c*, right column). The control parameters $\{p_1, p_2\}$ are represented in the upper left figure, while deformed configurations with positive/negative curvature at the fixed clamp are highlighted by blue/red dashed curve. At each stage, the clamp position at the previous stage and its path until then is highlighted. While two deformed configurations are possible for stages *a* and *b*, only one stable configuration exists at stage *c*.

During the experiments, photos were taken with a Sony $\alpha 9$ and videos with a high-speed camera (model *Sony PXW-FS5 4K*, 120 fps). A couple of videos showing example of use of the prototype as ECM-I and ECM-IIb are available as supplementary material.¹¹

Finally, the quantitative assessment of the theoretically predicted catastrophe loci is reported in Fig. 18 superimposing the experimental critical points for polikristal (star markers) and carbon fiber (crosses markers) rods. The following settings are shown: (i) ECMs-I (with $\kappa_R = 0.5$, $\lambda_R = 0.1$, $v = 0$, Fig. 18a, and with $\kappa_R = 0.5$, $\lambda_R = 0.3$, $v = 0$, Fig. 18b), (ii) ECM-IIb (case $\kappa_D = \lambda_D = \alpha = 0$, $\rho = 1$, $v = \pi$, Fig. 18c) and (iii) ECM-IIa (case $\kappa_D = \lambda_D = v = 0$, $\rho = 0.5$, $\alpha = \pi/4$, Fig. 18d). The comparisons reported in the figure fully display the experimental validation of the theoretical catastrophe loci. During the tests, very small portions of the catastrophe locus were not investigated because of some unavoidable physical limitations (for instance rod's self-intersection). The accuracy in the experimental measure of the critical conditions is observed to be higher when using carbon fiber rods. The inferior accuracy in testing with polikristal rods is expected to be related to the intrinsic viscosity and

¹¹Movies of experiments can be found in the additional material available at http://www.ing.unitn.it/~dalcorsof/elastica_catastrophe_machine.html

weight-stiffness ratio of the material.

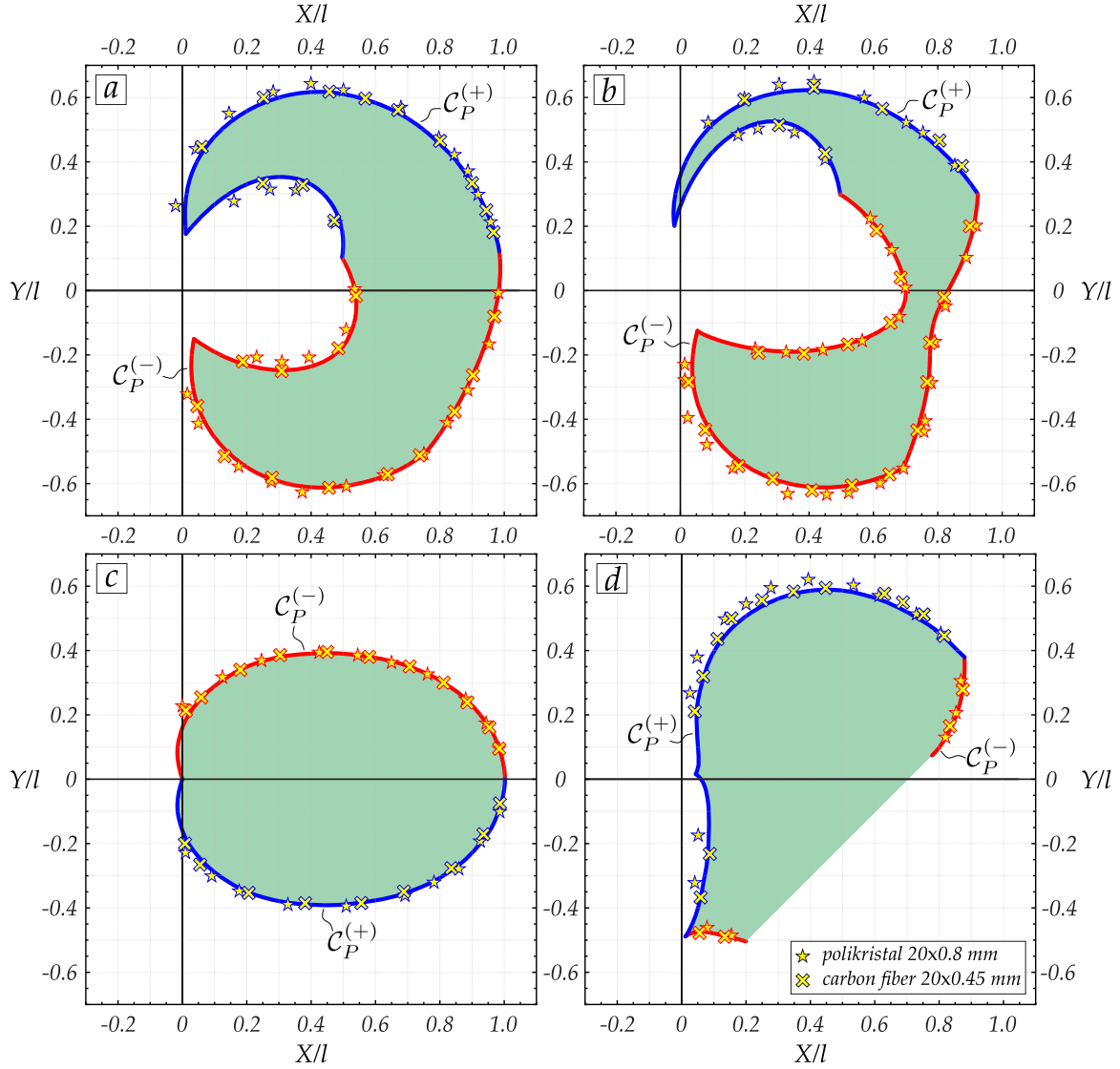


Figure 18: Experimental validation of the theoretically predicted catastrophe locus for ECMs-I (*a*: $\{\kappa_R = 0.5, \lambda_R = 0.1, v = 0\}$; *b*: $\{\kappa_R = 0.5, \lambda_R = 0.3, v = 0\}$), for ECM-IIb (*c*: $\{\kappa_D = \lambda_D = \alpha = 0, \rho = 1, v = \pi\}$), for ECM-IIa (*d*: $\{\kappa_D = \lambda_D = v = 0, \alpha = \pi/4, \rho = 0.5\}$). Measures from testing polikristal rod of thickness 0.8 mm (stars) and with a carbon fiber rod of thickness 0.45 mm (crosses) show an excellent agreement with the theoretical predictions.

6 Conclusions

For the first time, the design and the experimental validation of a catastrophe machine has been addressed for a system made up of a continuous and elastic flexible element, extending the classical formulation for discrete systems. A theoretical framework referring to primary kinematical quantities and exploiting the concept of the universal snap surface has been introduced. Among the infinite set of *elastica catastrophe machines*, two families have been proposed and the related catastrophe locus investigated to explicitly show the features of the

present model. A parametric analysis has disclosed substantial differences in the shape of the catastrophe locus in comparison with those deriving from classical catastrophe machines. In particular, the proposed machines can fulfil peculiar geometrical properties as convexity and a variable number of bifurcation points for the catastrophe loci. These meaningful characteristics may enhance the efficiency of snapping devices exploiting high-energy release points otherwise unreachable. The research has been completed by the validation of the theoretical results through the physical realization of a prototype enabling experiments with each of the two presented families of *elastica catastrophe machines*.

Acknowledgments AC and DM gratefully acknowledge financial support from the grant ERC advanced grant ‘Instabilities and nonlocal multiscale modelling of materials’ ERC-2013-AdG-340561-INSTABILITIES (2014-2019). FDC gratefully acknowledges financial support from the European Unions Horizon 2020 research and innovation programme under the Marie Skłodowska-Curie grant agreement INSPIRE - Innovative ground interface concepts for structure protection PITN-GA-2019-813424-INSPIRE. The authors are grateful to Mr. Lorenzo P. Franchini for the assistance during the experiments and to Prof. Claudio Fontanari (University of Trento) for a stimulating discussion.

References

- [1] Armanini, C., Dal Corso, F., Misseroni, D., Bigoni, D. (2017) From the elastica compass to the elastica catapult: an essay on the mechanics of soft robot arm. *Proc. R. Soc. A*, 473: 20160870.
- [2] Arnold, V.I. (1984) *Catastrophe Theory*. Springer Berlin Heidelberg.
- [3] Bertoldi, K., Vitelli, V., Christensen, J., van Hecke, M. (2017) Flexible mechanical metamaterials. *Nature Reviews* 2: 17066.
- [4] Bigoni, D. *Extremely Deformable Structures* - CISM Lecture Notes No. 562. Springer, 2015, ISBN 978-3-7091-1876-4, doi 10.1007/978-3-7091-1877-1.
- [5] Camescasse, B., Fernandes, A., Pouget, J. (2013) Bistable buckled beam: elastica modeling and analysis of static actuation. *Int. J. Sol. Struct.*, 50, 2881–2893.
- [6] Carricato, M., Parenti-Castelli, V., Duffy, J. (2001) Inverse static analysis of a planar system with flexural pivots. *J. Mech. Design* 123, 43–50
- [7] Carricato, M., Duffy, J., Parenti-Castelli, V. (2002) Catastrophe analysis of a planar system with flexural pivots. *Mech. Mach. Theory* 37(7), 693–716
- [8] Cazzolli, A., Dal Corso, F. (2019) Snapping of elastic strips with controlled ends. *Int. J. Sol. Str.* 162, 285–303
- [9] Chen, J. S., Lin, Y.Z. (2008). Snapping of a planar elastica with fixed end slopes. *ASME J. App.Mech.*, 75, 410241–410246.
- [10] Chen, J. S., Lin, W. Z. (2012). Dynamic snapping of a suddenly loaded elastica with fixed end slopes. *Int. J. Non-Linear Mech.*, 47, 489–495.
- [11] Cherepanov, G.P., Germanovich, L.N. (1993) An employment of catastrophe theory in fracture mechanics as applied to brittle strength criteria. *J. Mech. Phys. Solids* 41 (10), 1637–1649

- [12] Cohen, T., Givli, S. (2014) Dynamics of a discrete chain of bi-stable elements: A biomimetic shock absorbing mechanism. *J. Mech. Phys. Solids* 64, 426–439
- [13] Fargette, A., Neukirch, S., Antkowiak, A. (2014) Elastocapillary snapping: Capillarity induces snap-through instabilities in small elastic beams *Phys. Rev. Lett.*, 112, 137802
- [14] Fraternali, F., Carpentieri, G., Amendola, A. (2015) On the mechanical modeling of the extreme softening/stiffening response of axially loaded tensegrity prisms. *J. Mech. Phys. Solids* 74, 136–157
- [15] Gilmore, R. (1981) *Catastrophe Theory for Scientists and Engineers*. Dover
- [16] Groh, R.M.J., Pirrera, A. (2018) Generalised path-following for well-behaved nonlinear structures. *Computer Methods in Applied Mechanics and Engineering* 331, 394–426
- [17] Hines, R., Marsh, D., Duffy, J. (1998) Catastrophe Analysis of the Planar Two-Spring Mechanism *Int. J. Rob. Res.* 17(1), 89–101
- [18] Harne, R.L., Wang, K.W. (2013) A review of the recent research on vibration energy harvesting via bistable systems. *Smart Mat. Struct.* 22, 023001
- [19] Hunt, G. W. (1977) Imperfection-Sensitivity of Semi-Symmetric branching. *Proc. R. Soc. A* 357, 193–211
- [20] Kochmann, D., Bertoldi, K. (2017) Exploiting Microstructural Instabilities in Solids and Structures: From Metamaterials to Structural Transitions. *Appl. Mechanics Rev.*, 69, 050801
- [21] Lengyel, A., You, Z. (2004) Bifurcations of SDOF mechanisms using catastrophe theory. *Int. J. Sol. Struct.* 41, 559–568
- [22] O’Carroll, M.J. (1976) Fold and cusp catastrophes for critical flow in hydraulics. *Appl. Math. Modelling* 1, 108–109
- [23] Lu, T., Cheng, S., Li, T., Wang, T., Suo, Z. (2016) Electromechanical Catastrophe. *Int. J. Appl. Mechanics* 8, 164000
- [24] Nagy, P., Tasnadi, P. (2014) Zeeman catastrophe machines as a toolkit for teaching chaos. *Eur. J. Phys.* 35, 015018
- [25] Poston, T., Stewart, I. (1978) *Catastrophe Theory and Its Applications*. Pitman
- [26] Qin, S., Jiao, J.J., Wang, S., Long, H. (2001) A nonlinear catastrophe model of instability of planar-slip slope and chaotic dynamical mechanisms of its evolutionary process. *Int. J. Sol. Struct.* 38, 8093–8109
- [27] Raney, J.R., Nadkarni, N., Daraio, C., Kochmann, D.M., Lewis, J.A., Bertoldi, K. (2016) Stable propagation of mechanical signals in soft media using stored elastic energy. *Proc. Nat. Acad. Sci.* 113 (35) 9722–9727.
- [28] Sano, T.G., Wada, H. (2019) Twist-Induced Snapping in a Bent Elastic Rod and Ribbon, *Phys. Rev. Lett.* 122, 114301
- [29] Sano, T.G., Wada, H. (2018) Snap-buckling in asymmetrically constrained elastic strips, *Phys. Rev. E*, 97, 013002
- [30] Schioler, T., Pellegrino, S. (2007) Space Frames with Multiple Stable Configurations. *AIAA Journal*, 45 (7), 1740–1747.
- [31] Thom, R. (1969) Topological models in biology. *Topology* 8(3), 313–335
- [32] Thom, R. (1975) *Structural atability and morphogenesis*. W.A. Benjamin Inc.
- [33] Thompson, J.M.T. (1983) On the convection of a cusp in elastic stability. *J. Mech. Phys. Solids* 31 (3), 205–222

- [34] Woodcock, A.E.R., Poston, T.A. (1976) A higher catastrophe machine. *Proc. Cambridge Philos. Soc.* 79, 343–350
- [35] Yang, D., Mosadegh, B., Ainla, A., Lee, B., Khashai, F., Suo, Z., Bertoldi, K., Whitesides, G.M. (2015) Buckling of elastomeric beams enables actuation of soft machines. *Adv. Mater.* 27, 6323–6327
- [36] Yin, J.P., Marsh, D., Duffy, J. (1998) Catastrophe analysis of planar three-spring mechanism. Proc. of DETC 98, 1998 ASME Des. Eng. Tech. Conf., September 13–16, 1998, Atlanta, GA
- [37] Zeeman, E.C. (1972) A catastrophe machine. In *Towards a Theoretical Biology* (C. H. Waddington, ed.). Edinburgh University Press, Edinburgh. Vol. 4, 276–282
- [38] Zeeman, E.C. (1976) Catastrophe Theory. *Scientific American* 234, 65–83
- [39] Zeeman, E.C. (1977) Catastrophe Theory: Selected Papers, 1972–77. Addison-Wesley Educational Publishers
- [40] Zeeman, E.C. (1976) Euler buckling. In *Structural Stability, the theory of catastrophes, and applications in the sciences* (P. Hilton, ed.). Springer, Berlin, 373–395
- [41] Zunic, J., Rosin, P. L. (2004) A new convexity measure for polygons. *IEEE Transactions on Pattern Analysis and Machine Intelligence*, 26(7), 923–934.